AGU PUBLICATIONS

Geochemistry, Geophysics, Geosystems

RESEARCH ARTICLE
10.1002/2017GC006805

Observed correlation between the depth to base and top of gas hydrate occurrence from review of global drilling data

M. Riedel[1] and T. S. Collett[2]

[1]GEOMAR Helmholtz Centre for Ocean Research Kiel, Kiel, Germany, [2]US Geological Survey, Denver Federal Centre, Denver, Colorado, USA

Key Points:
- An inventory of 21 gas hydrate drilling campaigns is presented
- The top of gas hydrate occurrence and depth of gas hydrate stability are defined from drilling with uncertainties depending on proxy used
- Statistical relationships are developed to predict thickness of gas hydrate occurrence zone from depths of gas hydrate stability

Correspondence to:
M. Riedel,
mriedel@geomar.de

Citation:
Riedel, M., and T. S. Collett (2017), Observed correlation between the depth to base and top of gas hydrate occurrence from review of global drilling data, *Geochem. Geophys. Geosyst.*, *18*, 2543–2561, doi:10.1002/2017GC006805.

Received 6 JAN 2017
Accepted 1 JUN 2017
Accepted article online 9 JUN 2017
Published online 13 JUL 2017

Abstract A global inventory of data from gas hydrate drilling expeditions is used to develop relationships between the base of structure I gas hydrate stability, top of gas hydrate occurrence, sulfate-methane transition depth, pressure (water depth), and geothermal gradients. The motivation of this study is to provide first-order estimates of the top of gas hydrate occurrence and associated thickness of the gas hydrate occurrence zone for climate-change scenarios, global carbon budget analyses, or gas hydrate resource assessments. Results from publically available drilling campaigns (21 expeditions and 52 drill sites) off Cascadia, Blake Ridge, India, Korea, South China Sea, Japan, Chile, Peru, Costa Rica, Gulf of Mexico, and Borneo reveal a first-order linear relationship between the depth to the top and base of gas hydrate occurrence. The reason for these nearly linear relationships is believed to be the strong pressure and temperature dependence of methane solubility in the absence of large difference in thermal gradients between the various sites assessed. In addition, a statistically robust relationship was defined between the thickness of the gas hydrate occurrence zone and the base of gas hydrate stability (in meters below seafloor). The relationship developed is able to predict the depth of the top of gas hydrate occurrence zone using observed depths of the base of gas hydrate stability within less than 50 m at most locations examined in this study. No clear correlation of the depth to the top and base of gas hydrate occurrences with geothermal gradient and sulfate-methane transition depth was identified.

1. Introduction

Over the past two decades, numerous marine drilling expeditions were conducted to study gas hydrate occurrences, specifically with an aim to understand the geologic controls on the occurrence of gas hydrate and to understand their role as a future source of energy. Deep scientific drilling was performed on the southern and northern Cascadia margin, off India, China, Japan, South Korea, the eastern U.S. margin (Blake Ridge), and the U.S. Gulf of Mexico. The aim of our study presented here is to define (if present) first-order correlations between the top of gas hydrate occurrence zone (TGHOZ), base of gas hydrate stability zone (BGHSZ), and possibly any further correlations with the depth of the sulfate-methane transition zone (SMTZ), and derived geothermal gradients. To do so, we compiled data from 21 deep drilling expeditions (see details below). Some earlier attempts in combining such information is provided in *Booth et al*. [1996] or the compilation by the US Geological Survey [e.g., *Kvenvolden and Lorenson*, 2001].

In addition to the study of gas hydrates from an energy point of view, defining the global abundance of gas hydrate is also important to estimate their potential as natural hazards (to production or the environment) as well as for climate studies. In this context, the top of gas hydrate occurrence and the base of gas hydrate stability define the container size required to estimate the resource potential and thus the total amount of carbon stored in solid gas hydrates. The vulnerability of gas hydrate to climate change (e.g., a warming scenario) is linked to the overall burial depth below seafloor and overall water depth of the gas hydrate occurrence. The depth to which gas hydrate occurs in the sediment is further controlled by the geothermal gradient and methane concentrations in sediment pore waters at depth (see schematic diagram in Figure 1). Our compilation of deep drilling data, especially the top of gas hydrate occurrences as observed in core and log-data, may also be a useful asset for developing future gas hydrate drilling campaigns, especially with depth-limited devises such as seafloor drill rigs, or in regions where no previous drilling information on the extent of gas hydrates occurrences exist, and information about gas hydrates may be limited to seismic observations of a bottom-simulating reflector (BSR) as main indicator for the simple presence of gas hydrates in that region.

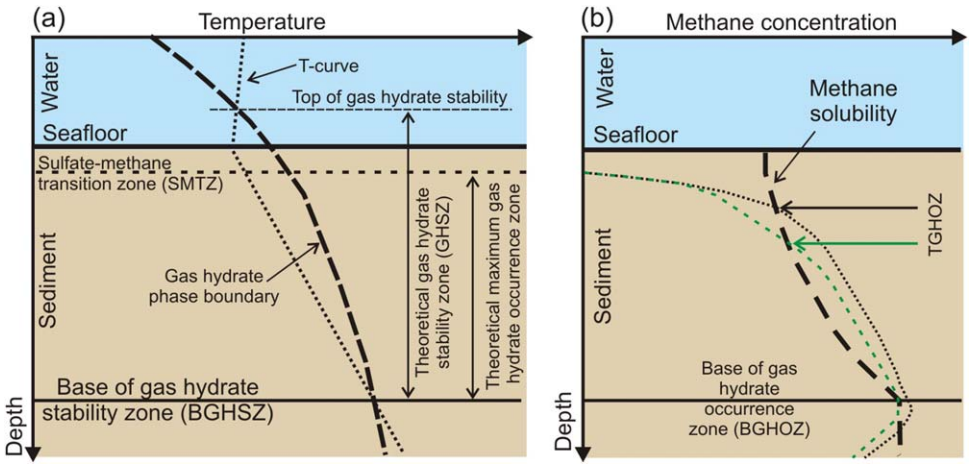

Figure 1. Schematic diagram for (a) gas hydrate phase boundary and (b) methane concentration (green dashed and black dotted lines are two simplified examples) and methane solubility. Identified are the depths of the sulfate-methane transition zone, top and base of gas hydrate stability zone, as well as the corresponding top and base of gas hydrate occurrence zone (TGHOZ, BGHOZ) for the two examples of methane concentration profiles. Depth is not plotted to scale.

The balance between pore water methane solubility (itself a function of temperature and pressure) and local methane concentrations is a critical factor in allowing the formation of gas hydrate, and local methane concentrations are influenced by in situ methane production (a function of total organic carbon available, as well as temperature), methane advection by fluid flow from greater depth, and sedimentation (burial) rates. Several authors have estimated the global abundance of gas hydrates [e.g., *Kvenvolden*, 1988; *Milkov*, 2003; *Klauda and Sandler*, 2005] or more local basin wide estimates (e.g., for the U.S. Gulf of Mexico by the *Minerals Management Service* [2008]) but global estimates vary over several orders of magnitude. Also, assessments conducted for energy assessments are not always directly comparable to those made for global methane abundance and climate studies (though technically mostly based on the same overall methodology) as described in *Boswell and Collett* [2011].

Other approaches for predicting gas hydrate abundance have been suggested, e.g., based on geochemical transport-reaction modeling [e.g., *Wallmann et al*., 2006], transfer functions based on measured pore fluid compositions [e.g., *Marquardt et al*., 2010] or coupled momentum, mass, and energy equations [e.g., *Xu and Ruppel*, 1999]. In all these analyses, either complex mathematical modeling needs to be performed or downhole pore fluid observations are required as verification of predicted concentrations. Several attempts have been previously suggested to calculate the vertical abundance of gas hydrate from the depth of the SMTZ and the shape of the down-core profiles of sulfate (and methane), as described, e.g., by *Paull et al*. [2005] and *Bhatnagar et al*. [2008, 2011]. Here data from shallow (piston/gravity) coring are used. The issues associated with these approaches are often impacted by a number of factors, including the limited nature of the gas being sourced mostly by microbial processes, controls on vertical (1-D) fluid migration, lack of incorporation of sediment-type controls on hydrate growth, and difficulties in the calibration of model-results with available drilling/core data.

In contrast, it may be possible to define a simpler approach to set critical boundaries to the potential size of the "gas hydrate stability container" (i.e., top and base of the stability field) if one can develop empirical relationships for these parameters from deep drilling observations. In order to investigate if such correlations may exist and how robust these may be, we have compiled data from 58 individual drill sites completed as part of 21 drilling campaigns in ten different geological regions, for which coring and/or geophysical logging programs were conducted (Figure 2).

The following drilling sites and margins were included in this study:

1. Cascadia Margin (active continental margin, accretionary prism):
   i. Ocean Drilling Program (ODP) Leg 146 [*Westbrook et al*., 1994],
   ii. Integrated Ocean Drilling Program (IODP) Expedition 311 [*Riedel et al*., 2006], and
   iii. ODP Leg 204 [*Tréhu et al*., 2003].

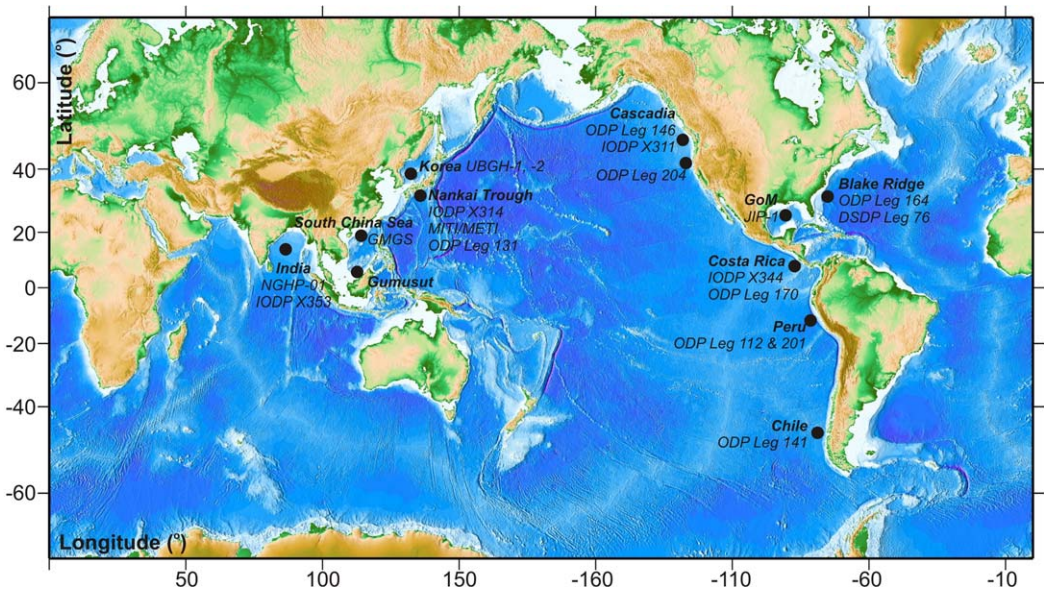

Figure 2. Map showing generalized locations of drilling campaigns utilized in this study. In each region, several drill sites are considered. For details, refer to Table 1 and references cited in text.

2. Blake Ridge (passive continental margin)
   i. ODP Leg 164 [*Paull et al*., 1996] and
   ii. DSDP Leg 76, Site 533 [*Sheridan et al*., 1983].
3. India East Coast (passive continental margin)
   i. India National Gas Hydrate Program Expedition 1, NGHP-01 [*Collett et al*., 2014; *Kumar et al*., 2014, and references therein] and
   ii. IODP Expedition 353, Sites U1445 and U1446 [*Clemens et al*., 2016].
4. Korea (back-arc basin)
   i. Ulleung Basin Gas Hydrate Drilling Program, UBGH-1 and −2 [*Park et al*., 2008; *Ryu et al*., 2013, and references therein].
5. Costa Rica Margin (active continental margin, erosive sedimentary prism)
   i. IODP Expedition 344, Site U1412 [*Harris et al*., 2013] and
   ii. ODP Leg 170 [*Kimura et al*., 1997].
6. Borneo (passive continental margin)
   i. Gumusut drilling project [*Paganoni et al*., 2016].
7. Peru (active continental margin, accretionary prism)
   i. ODP Leg 201, Site 1230 [*D'Hondt et al*., 2003] and
   ii. ODP Leg 112, Sites 685 and 688 [*Suess et al*., 1988].
8. Gulf of Mexico (passive continental margin)
   i. Joint Industry Project, Keathley Canyon KC151 [*Ruppel et al*., 2008, and references therein].
9. South China Sea (passive continental margin)
   i. Sites SH-2, −3, and −7 [e.g., *Matsumoto et al*., 2011, and references therein; *Wang et al*., 2011a, 2011b, 2014a, 2014b; *Wu et al*., 2011].
10. Japan, Nankai Trough (active continental margin, accretionary prism)
    i. ODP Leg 131, Site 808 [*Taira et al*., 1991],
    ii. MITI Wells [*Tsuji et al*., 2004; *Matsumoto*, 2008],
    iii. METI Wells, α-1 and β-1 well [*Takeuchi and Matsumoto*, 2009], and
    iv. IODP Expedition 314, Site C0002 [*Miyakawa et al*., 2014].
11. Chile (active continental margin, erosive prism
    i. ODP Leg 141, Sites 859, 860, and 861 [*Behrmann et al*., 1992].

It is important to note that coring operations with modern detection techniques such as infrared (IR) core imaging, which has been used since ODP Leg 201 [*Ford et al*., 2003] and ODP Leg 204 [*Weinberger et al*., 2005]

have allowed more careful analyses of sites cored in the past ~15 years compared to earlier such undertakings. When discussing statistical relationships between depths of gas hydrate occurrences and other parameters (as outlined below), the relative vintage of the data from expeditions conducted during earlier drilling campaigns such as DSDP Leg 76 [*Sheridan et al*., 1983] and ODP Leg 112 [*Suess et al*., 1988] should be considered with an overall larger degree of uncertainty (as discussed later).

In the context of this study, we strictly use the structure I gas hydrate phase boundary and ignore occurrences of higher hydrocarbons that may generate structure II gas hydrates. Thus, the term BGHSZ is to be interpreted as base of structure I gas hydrate, or in line with previous suggested terminology, BS_IGHSZ [e.g., *Boswell et al*., 2016; *Paganoni et al*., 2016]. We further want to emphasize that our study is not concerning the detailed and local gas hydrate concentrations with depth and any localized variations therein. As the drilling of gas hydrate over the past decades has shown a high degree of intrasite variability (e.g., during ODP Leg 204 [*Tréhu et al*., 2004] or IODP Expedition 311 [*Riedel et al*., 2006]) such details are not considered for this study.

2. Data, Methods, and Uncertainties

The detection of gas hydrate can be made either directly through visual observations of the core or by indirect observations and the use of proxy measurements as compiled in *Riedel et al*. [2010]. Data used for our inventory are from offshore drilling campaigns that span the time from as early as 1983 with DSDP Leg 76 [*Sheridan et al*., 1983] to IODP Expedition 353 off India conducted in 2015 [*Clemens et al*., 2016]. The proxies used in this study include core-based proxies such as pore water freshening in the form of reduced chlorinity as shown in Figure 3a and described first by *Hesse and Harrison* [1981], significant cold spots in IR images of cores just after recovery (Figure 3b) [e.g., *Long et al*., 2010], soupy or mousse-like textures of sediments [e.g., *Kastner et al*., 1995; *Pinero et al*., 2007] (Figure 3b), logging-based proxies compiled by *Collett and Lee* [2012] such as formation-responses above a (site-specific) background trend in either electrical resistivity (Figure 3c), *P* and *S* wave velocity, or sonic wave attenuation or pressure-core-derived methane concentrations (Figure 3d) [*Schultheiss et al*., 2010].

Log-data used in this study are either from conventional wireline (WL) deployments where data are acquired after a hole has been drilled or logging-while-drilling (LWD) techniques, where data are acquired at the same time as the hole is advanced. Differences in these two principle logging-techniques and their relevance to detecting and quantifying gas hydrates are described by *Collett and Lee* [2012] or *Goldberg et al*. [2010].

Overall, substantial differences exist between the various methods to detect gas hydrate and each method bears its own uncertainty. Uncertainties in defining the occurrence of gas hydrate based on data from recovered sediment cores is often challenged by the quality of the recovered cores and the extent of core coverage over the depth interval of interest. Incomplete core recovery, spot-coring approaches, core-expansion after recovery from sediment pore water degassing (often augmented by gas hydrate dissociation during core recovery) all lead to a significant uncertainty in assigning depth values to acquired core measurements. Prior to the use of IR-guided core sampling to identify cold spots associated with dissociating gas hydrate, pore fluid-based detection of gas hydrate was purely a hit-and-miss undertaking. The presence of gas hydrate can be inferred through observations of the core and using typical textures as proxies (soupy or mouse-like sediment disturbances). Thus, only continuous coring and exploitation of all core-based proxies can lead to a robust definition of the top of gas hydrate occurrence zone. However, the time gap between core recovery, examination in the core recovery lab, and IR scanning can influence the detection of gas hydrate [*Weinberger et al*., 2005]. Moreover, if a gas hydrate occurs close to the center of the core, the IR cold spot anomaly may only be seen after some additional time has lapsed to allow for more complete hydrate dissociation and associated conduction of the temperature anomaly to reach the outer core liner, where it can be imaged with the IR camera. Here secondary scans and/or comparisons with core-textures may help to better infer the presence of gas hydrates [*Long et al*., 2010]. However, the lower limit of the ability of IR scanning (or the development of significant disturbed sediment textures) to detect gas hydrate dissociation is not known and is largely dependent on the experience of the individual(s) performing the analysis as well as and ambient conditions during the IR scanning (such as outside air temperature, sun light conditions, humidity, core-liner material, and handling of the core prior to scanning).

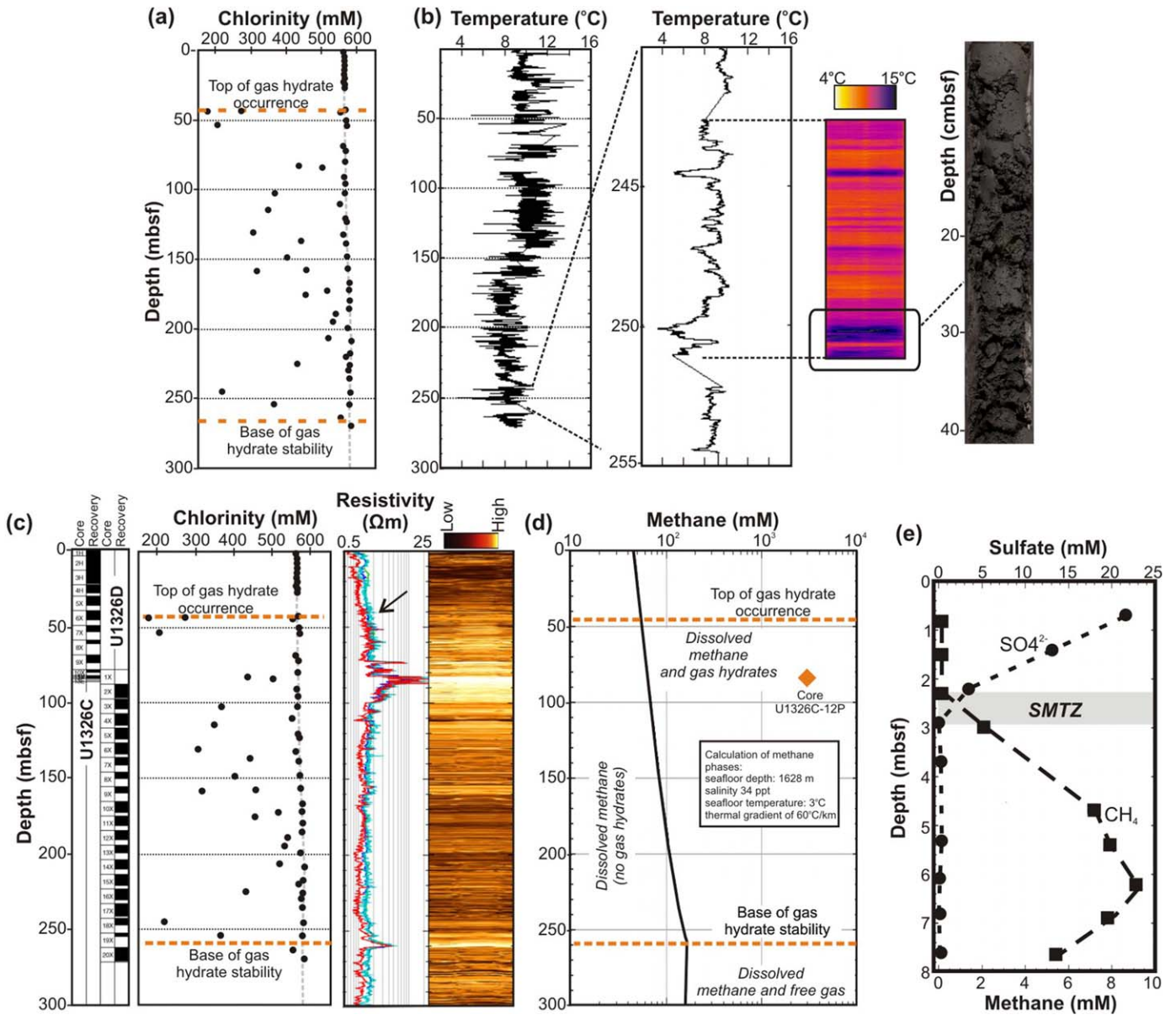

Figure 3. Examples of determining gas hydrate occurrence from (a) pore water chlorinity freshening and (b) core-IR imaging in combination with soupy and/or mouse-like sediment textures, (c) log-data responses using electrical resistivity anomalies relative to background as the main indicator for the presence of gas hydrate with Figure 3d, supporting evidence from pressure-core-derived gas hydrate concentrations. Also shown are the core recovery plots to show how incomplete core recovery may hamper definition of top and base of gas hydrate occurrence from core-based data. Definition of the depth of the sulfate-methane transition zone (SMTZ) from sulfate and methane data is shown in Figure 3e. All images are based on data from Site U1326, IODP Expedition 311 [*Riedel et al*., 2006].

Using logging-based proxies in defining the occurrence of gas hydrates also holds a variety of uncertainties, including the nature of the physical measurement made by the logging tool and its ability to provide robust measures for detecting gas hydrate, the logging-technique (LWD or WL), speed of logging, borehole conditions, logging tools, and drilling-fluid used. Ship heave-compensation is usually robust enough to compensate for any ship-motion, so depth uncertainties associated with downhole log-data are generally rare and are usually associated with the selection and/or use of an incorrect reference datum such as inaccurately picking the depth of the seafloor from the acquired logs. In general, the vertical resolution of WL tools is higher (few centimeters) than LWD tools (tens of centimeters), but for the most part both logging-techniques yield relatively high resolution analysis of the occurrence of gas hydrate. By comparison, LWD data can be acquired from the seafloor to the bottom of the drilled hole, but WL data cannot usually be obtained from the upper 30–90 m of each well logged because of borehole stability problems; thus, limiting

AGU Geochemistry, Geophysics, Geosystems 10.1002/2017GC006805

Table 1. Global Data Base of Drilling-Derived Values in Top of Gas Hydrate Occurrence Zone (TGHOZ), Base of Gas Hydrate Stability Zone (BGHSZ), Sulfate-Methane Transition Zone (SMTZ) and Geothermal Gradients[a]

Site Location	SMTZ (mbsf)	TGHOZ (mbsf)	BGHSZ (mbsf)	Water Depth (m)[b]	Thermal Gradient (°C/km)	BGHSZ (mbsl)	TGHOZ (mbsl)	Thickness GHOZ (m)	Predicted TGHOZ (mbsf) Equation (1)	Predicted TGHOZ (mbsf) Equation (2)	Difference (m) Equation (1)	Difference (m) Equation (2)	Reference
Cascadia Margin													
IODP X311													
1325	4.5 ± 1	73 ± 5[c] (Cl^-)	245 ± 17[d]	2201 ± 1	60 ± 3	2446 ± 18	2274 ± 6	172 ± 22	86.4	138.8	13.4	33.7	*Riedel et al.* [2006, 2010]
1326	2.5 ± 1	47 ± 1[e] (Cl^-)	261 ± 2[d]	1828 ± 1	n.d.	2089 ± 3	1875 ± 2	214 ± 3	117.2	150.1	70.2	63.9	
1327	8 ± 1	111 ± 1 (LWD res.)	230 ± 8[d]	1322 ± 1	55 ± 4	1552 ± 9	1433 ± 2	119 ± 9	108.4	127.2	−2.6	−8.2	
1329	9 ± 1	n.d.	125 ± 3[d]	960 ± 1	72 ± 4	1085 ± 4	n.d.	n.d.	n.d.		n.d.		
ODP Leg 204													
1244	8.5 ± 1	45 ± 1[e] (IR, Cl^-)	125 ± 3	907 ± 1	60 ± 1	1032 ± 4	952 ± 2	80 ± 4	25.0	49.8	−20.0	30.2	*Tréhu et al.* [2003]
1246	7 ± 1	40 ±1[e] (IR, Cl^-)	114 ± 2	860 ± 1	61 ± 2	974 ± 3	900 ± 2	74 ± 3	16.4	41.7	−23.6	32.3	
1247	12 ± 1	45 ± 1[e] (IR, Cl^-)	122 ± 3	845 ± 1	52 ± 1	967 ± 4	890 ± 2	77 ± 4	24.7	47.6	−20.3	29.4	
1251	4.5 ± 1	90 ± 1[e] (IR, Cl^-)	197.5 ± 5	1220 ± 1	53 ± 1	1420 ± 6	1310 ± 2	110 ± 6	83.9	105.1	−6.1	4.9	
1245	7 ± 1	51 ± 1[e] (IR, Cl^-)	136 ± 7.8	880 ± 1	55 ± 1	1014 ± 8.8	931 ± 2	83 ± 8.8	34.7	56.4	−16.3	26.6	
1252	5 ± 1	43 ± 1[e] (IR, Cl^-)	170 ± 5	1040 ± 1	59 ± 4	1210 ± 6	1083 ± 2	127 ± 6	62.6	83.0	19.6	44.0	
Blake Ridge													
ODP Leg 164													
994	20.5 ± 1	195 ± 1.5[f] (Cl^-)	428 ± 5	2798 ± 1	36.4 ± 1.3	3236 ± 6	2993 ± 2.5	233 ± 6.5	237.1	273.2	42.1	−40.2	*Paull et al.* [1996]
995	21 ± 1	190 ± 1.5[f] (Cl^-)	450 ± 10	2777.7 ± 1	33.5 ± 0.9	3238 ± 11	2978 ± 2.5	260 ± 11.5	258.6	289.4	68.6	−29.4	
997	23 ± 1	210 ± 1.5[f] (Cl^-)	451 ± 8	2770 ± 1	36.4 ± 1.3	3221 ± 9	2980 ± 2.5	241 ± 9.5	260.3	290.1	50.3	−49.1	
DSDP													
533	22 ± 5[g]	247 ± 4[h]	600 ± 5	3191 ± 1	36.0[i]	3791 ± 6	3438 ± 5	353 ± 9	385.7	400.0	138.7	−47.0	*Sheridan et al.* [1983]
India													
NGHP-1													
1–3	10 ± 1	165 ± 2[f] (IR, Cl^-)	200 ± 5	1076 ± 1	39 ± 2	1276 ± 6	1241 ± 3	35 ± 7	89.9	105.1	−75.1	−70.1	*Collett et al.* [2014] and
1–5	21 ± 1	70.4 ± 4[f] (Cl^-)	130 ± 4	945 ± 1	44 ± 3	1075 ± 5	1017 ± 5	56.6 ± 8	28.2	53.5	−42.2	6.1	references therein
1–7	32 ± 1	61 ± 1 (LWD res.)	193.5 ± 5	1285 ± 1	52 ± 2	1478.5 ± 6	1346 ± 2	132.5 ± 6	75.0	100.3	14.0	32.2	
1–14	22 ± 1	52 ± 4[f] (Cl^-)	129.5 ± 20[j]	895 ± 1	38 ± 2	1024.5 ± 21	947 ± 5	77.5 ± 24[j]	29.8	53.1	−22.2	24.4	
1–17	25 ± 1	260 ± 1[f] (IR, Cl^-)	614 ± 6	1344 ± 1	19 ± 2	1958 ± 7	1604 ± 2	354 ± 7	475.6	410.3	215.6	−56.3	
1–18	20 ± 1	112 ± 1[f] (IR, mous.)	215 ± 2.5	1374 ± 1	50 ± 2[k]	1589 ± 3.5	1486 ± 2	103 ± 3.5	91.9	116.1	−20.1	−13.1	
1–19	21 ± 1	98 ± 8[f] (Cl^-)	195 ± 7.5	1422 ± 1	53 ± 2	1617 ± 8.5	1520 ± 9	97 ± 15.5	70.7	101.4	−27.3	−4.4	
1–20	14 ± 1	45 ±1[f] (IR, Cl^-)	195 ± 15[j]	1146 ± 1	49 ± 2[k]	1341 ± 16	1191 ± 2	150 ± 16	82.2	101.4	37.2	48.6	
1–6	n.d.	110 ± 1[f] (IR, Cl^-)	210 ± 5	1160 ± 1	n.d.	1370	1270	100 ± 6	96.0	112.5	−14.0	−12.5	
1–4	n.d.	80 ± 1 (LWD res.)	182 ± 5	1081 ± 1	n.d.	1263 ± 6	1161 ± 2	102 ± 6	72.4	91.8	−7.6	10.2	
1–2	n.d.	58 ± 1 (LWD res.)	170 ± 5	1058 ± 1	n.d.	1228 ± 6	1116 ± 2	112 ± 6	61.8	83.0	3.8	29.0	
1–8	n.d.	n.d.	257 ± 5	1689 ± 1	n.d.	1946 ± 6	n.d.	n.d.	n.d.		n.d.		
1–9	n.d.	n.d.	290 ± 5	1946 ± 1	n.d.	2236 ± 6	n.d.	n.d.	n.d.		n.d.		
X353													
1445	17 ± 1	31 ±1[f] (IR, Cl^-)	n.d.	2502 ± 1	50 ± 2[k]	n.d.	2533 ± 2	n.d.	n.d.		n.d.		*Clemens et al.* [2016]
1446	20 ± 1	125 ± 1[f] (IR, Cl^-)	247.5 ± 7.5[l]	1430 ± 1	50 ± 2[k]	1677.5 ± 8.5	1555 ± 2	122.5 ± 8.5	120.7	90.3	−116.2	−65.3	
Korea													
UBGH													
2–1_1	7.7 ± 1	94 ±1[f] (IR, Cl^-)	165 ± 2[j]	1534 ± 1	100 ± 2[k]	1699 ± 3	1628 ± 2	71 ± 3	37.3	79.3	−56.7	−8.3	*Ryu et al.* [2013] and
2–1_2	n.d.	70 ± 1[f] (LWD res.)	165 ± 5[l]	1498 ± 1	Assumed	1663 ± 6	1568 ± 2	95 ± 6	38.8	79.3	−31.2	15.7	*Bahk et al.* [2013]
2–4	n.d.	140 ± 1[f] (LWD res.)	183 ± 5[l]	2156 ± 1	Assumed	2339 ± 6	2296 ± 2	43 ± 6	28.8	92.6	−111.2	−49.6	
2–6	6.5 ± 1	112 ± 1[f] (IR, Cl^-)	172.5 ± 2.5	2152 ± 1	112 ± 2[k]	2322 ± 3.5	2264 ± 2	58 ± 3.5	16.5	83.0	−95.5	−25.0	
2–8	n.d.	75 ± 1[f] (LWD res.)	165 ± 5[l]	1988 ± 1	Assumed	2153 ± 6	2063	90 ± 6	18.5	79.3	−56.5	10.7	
2–9	6.7 ± 1	95 ± 1 (LWD res.)	164 ± 5	2106 ± 1	115 ± 2[k]	2266 ± 6	2201 ± 2	65 ± 6	8.9	75.6	−86.1	−10.6	
2–5	8.2 ± 1	40 ± 1[f] (IR)	184 ± 3	1974 ± 1	96 ± 2[k]	2158 ± 4	2014 ± 2	144 ± 4	37.3	93.3	−2.7	50.7	
1–4	n.d.	155 ± 1[f] (IR, Cl^-)	180 ± 5[l]	1845 ± 1	Assumed	2025 ± 6	2000	25 ± 6	38.8	90.3	−116.2	−65.3	*Park et al.* [2008]
Borneo/Gumusut													
DC_E	n.k.	105 ± 1[f] (Cl^-)	155 ± 5	948.5 ± 1	63 ± 2[k]	1103.5 ± 6	1053.5 ± 2	50 ± 6	52.0	71.9	−53.0	−21.9	*Paganoni et al.* [2016]
South China Sea													
SH-7	17 ± 1	135± 1[f] (Cl^-)	181 ± 3	1105 ± 1	n.k.	1283 ± 4	1240 ± 2	43 ± 4	67.6	88.9	−67.4	−45.9	*Wang et al.* [2011a,b,a,b]
SH-2	25 ± 1	185 ± 1[f] (Cl^-)	251 ± 17[j]	1230 ± 1	45.6 ± 2[k]	1475 ± 18	1415 ± 2	60 ± 18	126.6	138.3	−58.4	−78.3	and *Wu et al.* [2011]
SH-3	22 ± 1	70 ± 1[f] (Cl^-)	206 ± 2	1240 ± 1	n.k.	1446 ± 3	1310 ± 3	136 ± 3	88.8	109.5	18.8	26.5	
Japan Nankai Trough													
Alpha-1	23 ± 1	100 ± 1[f] (Cl^-)	200 ± 2	730 ± 1	n.k.	930 ± 3	830 ± 2	100 ± 3	104.2	4.2	105.1	−5.1	*Takeuchi and Matsumoto*
Beta-1	7 ± 1	105 ± 0.5[f] (Cl^-)	337 ± 2	997 ± 1	43 ± 2[k]	1334 ± 3	1102 ± 1.5	232 ± 2.5	224.5	119.5	206.1	25.9	[2009]
MITI Well 1	n.d.	175 ± 1[f]	268 ± 1	945 ± 1	43 ± 2[k]	1213 ± 2	1141 ± 2	93 ± 2	160.5	−14.5	155.2	−62.2	*Matsumoto* [2008]
C0002 (X314)	n.k.	220 ± 10[m] (LWD res.)	400 ± 10	1964 ± 1	50 ± 2[k]	2364 ± 11	2184 ± 11	180 ± 20	244.8	24.8	252.5	−72.5	*Miyakawa et al.* [2014]

AGU Geochemistry, Geophysics, Geosystems

10.1002/2017GC006805

Table 1. (continued)

Site Location	SMTZ (mbsf)	TGHOZ (mbsf)	BGHSZ (mbsf)	Water Depth (m)[b]	Thermal Gradient (°C/km)	BGHSZ (mbsl)	TGHOZ (mbsl)	Thickness GHOZ (m)	Predicted TGHOZ (mbsf) Equation (1)	Predicted TGHOZ (mbsf) Equation (2)	Difference (m) Equation (1)	Difference (m) Equation (2)	Reference
Site 808	10 ± 1	110 ± 25[n]	205 ± 10	4841 ± 1	111.6 ± 10	5046 ± 11	4951 ± 26	95 ± 35	−61.3	−61.3	108.8	−13.8	*Taira et al.* [1991]
GoM-JIP1													
KC151#2	10 ± 1	100 ± 1[f] (Cl^-, LWD res.)	392 ± 2	1321.8 ± 1	n.k.	1713.8 ± 3	1421.8 ± 2	292 ± 3	263.7	246.6	163.7	45.4	*Ruppel et al.* [2008] and references therein
Costa Rica													
IODP X344													
1412	14.7 ± 1	71.6 ± 1[f] (Cl^-)	187 ± 5	1921 ± 1	85 ± 2[k] (114[o])	2108 ± 2	1992 ± 2	115.4 ± 2	42.4	95.5	−29.2	19.9	*Harris et al.* [2013]
Leg 170													
1040	20 ± 2	90 ±5[f] (Cl^-)	n.d.	4177 ± 1	7.2 ± 2[k]	n.d.	4267 ± 6	n.d.	n.d.		n.d.		*Kimura et al.* [1997]
1041	15 ± 2	116.7 ± 5[f] (Cl^-)	n.d.	3317 ± 1	22 ± 2[k]	n.d.	3433.7 ± 6	n.d.	n.d.		n.d.		
Peru													
ODP Leg 201													
1230	8 ± 1	71.6 ± 3[f] (Cl^-)	610± 50[j]	5086 ± 1	34.3 ± 2[k]	5696 ± 51	5159 ± 4	537 ± 53	316.8	243.8	407.3	129.7	*D'Hondt et al.* [2003]
ODP Leg 112													
685	12 ± 2	99 ± 20[f]	610 ± 50[j]	5070 ± 1	34.3 ± 2[k]	5680 ± 51	5169 ± 21	511 ± 70	317.5	218.5	407.3	103.7	*Suess et al.* [1988]
688	10 ± 2	135 ± 20[f]	500 ± 50[j]	3820 ± 1	52 ± 2[k]	4320 ± 51	3955 ± 21	365 ± 70	263.8	326.3	128.8	38.7	
682	n.d.	n.d.	477 ± 50[j]	3790 ± 1	49 ± 2[k]	4267 ± 51	n/a	n/a	n.d.		n.d.		
683	16 ± 2	n.d.	n.d.	3072 ± 1	50 ± 2[k]	n/a	n/a	n/a	n.d.		n.d.		
Chile													
ODP Leg 141													
859	<5[i]	30 ± 10[f] (Cl^-)	80 ± 10	2741 ± 2	190 ± 2[k]	2821 ± 12	2771 ± 11	50 ± 20	−94.1	16.6	−124.1	33.4	*Behrmann et al.* [1992]
860	<10[l]	n.d.	158 ± 10	2320 ± 2	106.4 ± 2[k]	2478 ± 12	n.d.	n.d.	n.d.		n.d.		
861	<12[i]	n.d.	250 ± 20	1658 ± 2	53.5[l]		n.d.	n.d.	n.d.		n.d.		

[a]Also indicated are the types of proxy used for detection onset of gas hydrates (Cl^-: pore water chlorinity freshening, IR: infrared imaging, mous.: mousse-like sediment texture, LWD rest.: Logging-while-drilling resistivity anomaly) as well as uncertainties in the depth values. These uncertainties are a function of the proxy used to define the parameters as well as core recovery through the interval of hydrate occurrences. n.d.: not determined and n.k.: not known to authors.

[b]Uncertainties reported are rounded to the nearest meter and are from determining average values from all available measurements at the drill site (which can include some or all of driller's depth, acoustic depth ranging, seismic depth, or ROV dive-depths).

[c]Uncertainty is based on poor core recovery in that interval.

[d]Uncertainty is based on *Riedel et al.* [2010, Table 1], where the BGHSZ was defined from various borehole measurements, core-analyses, thermal gradients, and seismic data.

[e]Uncertainty of 1 m is used for intervals with good/high core recovery, where gas expansion voids and sediment extrusion results in up to 1 m depth uncertainty postcuration.

[f]Uncertainty is defined by sample spacing.

[g]Uncertainty is defined by range of observations given in Table 4 of DSDP Vol. 76, p. 61.

[h]Uncertainty is defined by range of observations given in Table 1 of DSDP Vol. 76, p. 48.

[i]No uncertainty reported in literature, and no new uncertainty was defined.

[j]Uncertainty from discrepancy between thermal data and seismic observations.

[k]Uncertainty assumed; only one or two data points acquired, so no regression was attempted.

[l]Uncertainty from unknown velocity to convert bottom-simulating reflector (BSR) depths from seismic data to depth below seafloor.

[m]Uncertainty from a broad zone of elevated resistivity values in LWD data.

[n]Uncertainty from one recovered gas hydrate piece in wash core 131–808F-4W.

[o]The reported value of 114°C/km by *Harris et al.* [2013] is based on few values in the upper 35 mbsf. Using the seismically defined depth of the BSR (190 mbsf) and a seafloor temperature of 2.25°C, yields a geothermal gradient of ~85°C/km for the expected temperature at the phase boundary as defined for a seawater (34 ppt) and pure methane mix.

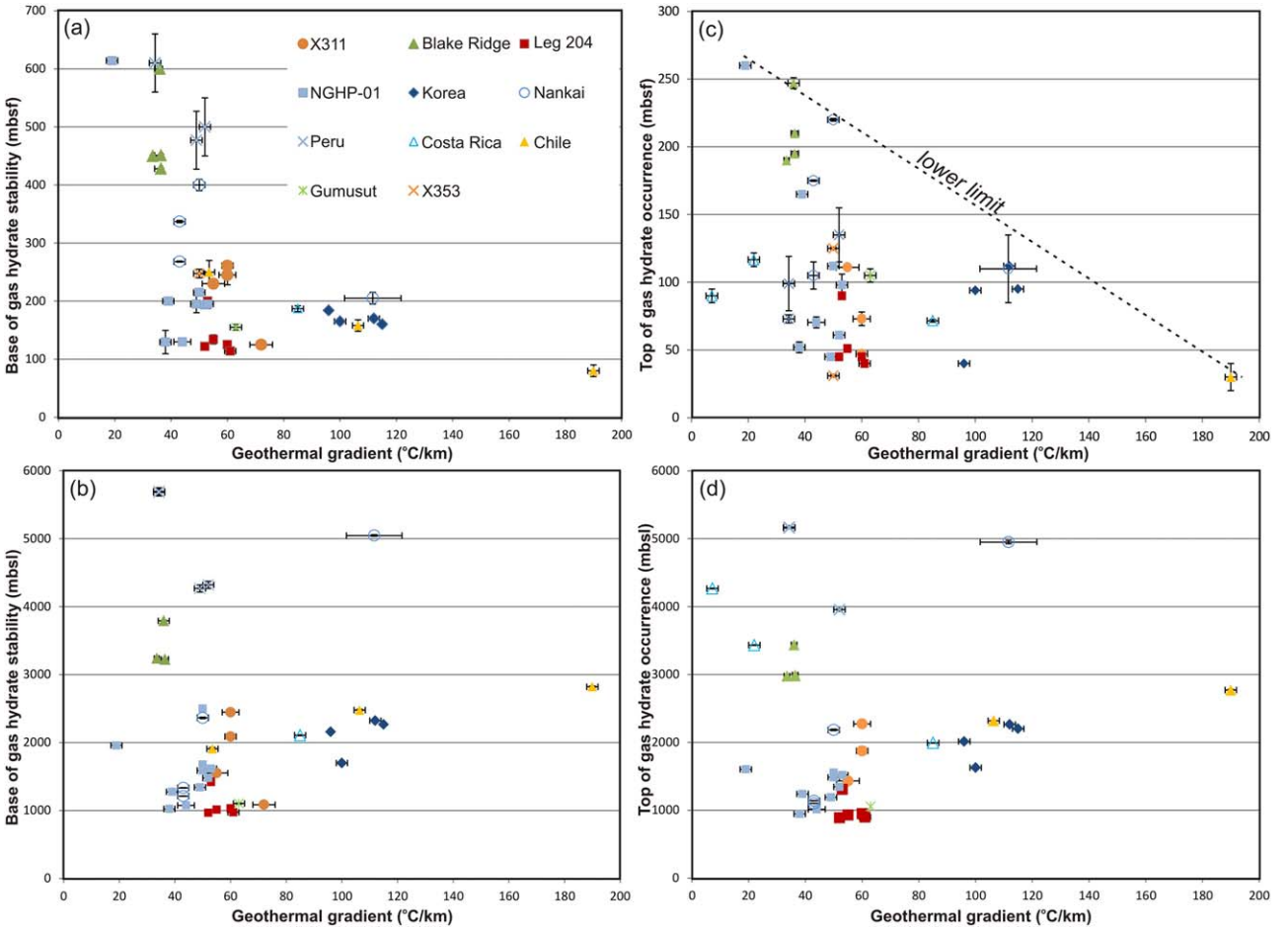

Figure 4. Correlations between geothermal gradient and (a, b) base of gas hydrate stability zone, and (c, d) top of gas hydrate occurrence (each shown in meters below seafloor (mbsf) in the upper panel, and meters below sea level (mbsl) in lower panel). Data from drilling campaigns are used where the geothermal gradients were determined by in situ measurements. Colors and symbols used in all subfigures are shown in the legend.

the coverage of WL acquired log-data. Detecting gas hydrates from the formation response using logged physical properties such as electrical resistivity, *P* or *S* wave velocity, or acoustic wave attenuation, requires establishing a site-dependent background trend in these physical properties, which are a function of porosity, in situ pore fluid composition, and bulk density of the formation (e.g., occurrence of authigenic carbonates). Additional influence on the ability to detect gas hydrate is the mode of occurrence (i.e., pore-filling, forming as veins, or massive nodules) and the sensitivity of the tool and measurement technique to anisotropy.

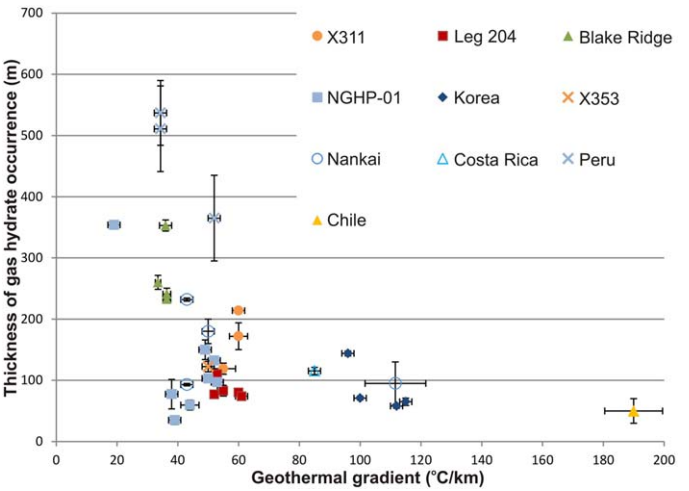

Figure 5. Crossplot of measured geothermal gradients and measured thickness of the gas hydrate occurrence zone (uncertainties see Table 1).

The depth of the sulfate-methane transition zone (SMTZ) in marine sediments is based on the measurement of sulfate and methane concentrations in recovered sediment core (Figure 3e). As the term SMTZ implies, this is a zone of some thickness, not necessarily

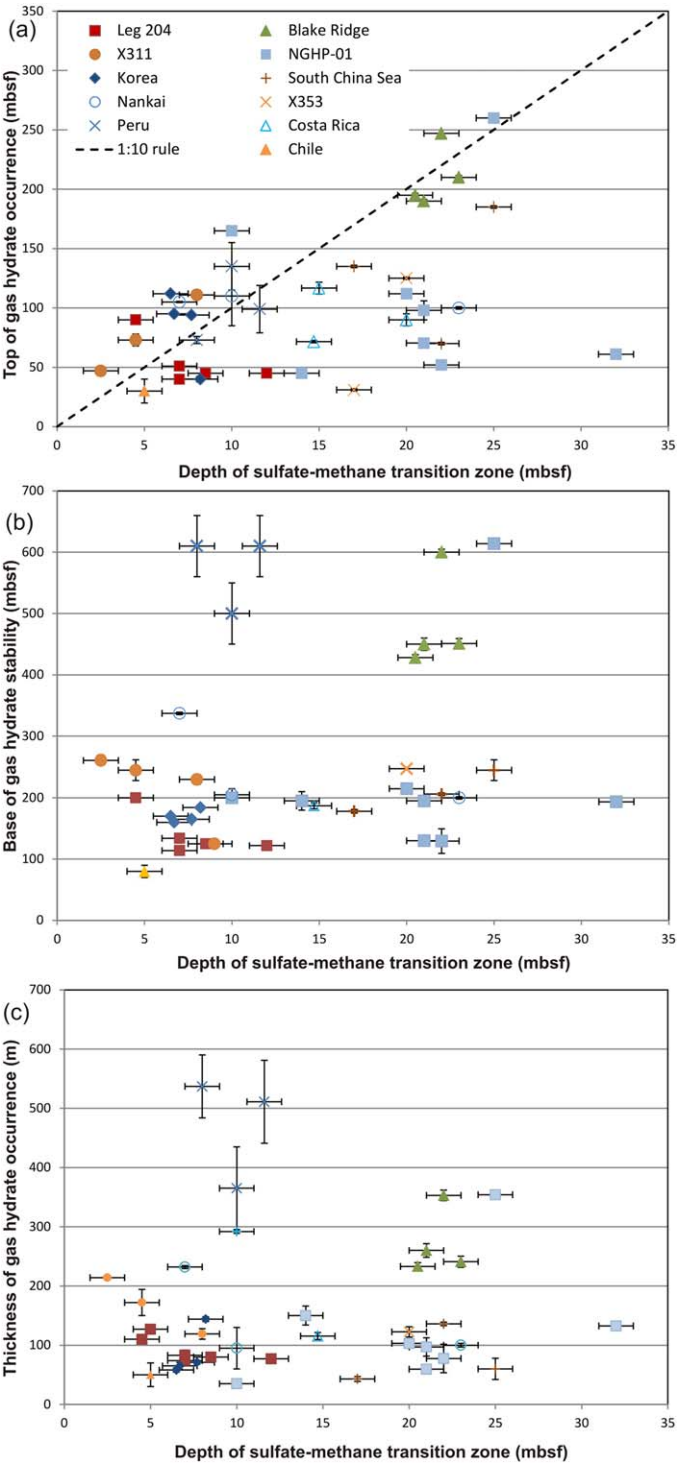

Figure 6. Correlation between the sulfate-methane transition zone depth and (a) the top of gas hydrate occurrence, (b) depth of the base of gas hydrate stability, and (c) thickness of the gas hydrate occurrence zone as measured from sites of 12 drilling campaigns (colors and symbols defined in legend). Data and uncertainties for each site are reported in Table 1 (references see text).

with a sharp boundary. We assign an uncertainty of ±1 m to the depth values of SMTZ reported in Table 1, which includes the uncertainty associated with defining the seafloor. Using the "mud-line core" to define seafloor and all subsequent depths as meters below seafloor (mbsf) can have some error usually due to the fact that the seafloor itself is not always captured in the core.

Defining geothermal gradients requires reliable measurements of temperature within the sediment column and at the seafloor. Data reported here from ODP and IODP drilling expeditions often utilize temperature measurements during piston coring [e.g., *Heesemann et al.*, 2006] or by using special wireline deployed tools mechanically inserted into the sediments, such as the Davis-Villinger Temperature probe [*Davis et al.*, 1997]. Other similar industry tools have been used during commercial drilling campaigns in the South China Sea [e.g., *Wang et al.*, 2014a], Ulleung Basin [e.g., *Ryu et al.*, 2013], or off Borneo [*Paganoni et al.*, 2016]. While each individual temperature measurement may yield a highly accurate temperature value, the temperature gradient is derived from the statistical analysis of individual tool derived values. Fundamentally, the assumption in all these regression analyses is a linear extrapolation of the geothermal gradient through the gas hydrate occurrence zone; which might not always be a correct assumption. Uncertainties in the values reported in Table 1 may be significant, but is not always provided with the reported data.

Overall, when comparing the ability of defining the top of gas hydrate occurrence zone from core-based proxies and direct observations or log-based methods, the core-based analyses are more reliable, especially in case of continuous coring. Core-based techniques allow physical testing of samples, whereas remote sensing relies on many assumptions (e.g., physical properties for the background hydrate-

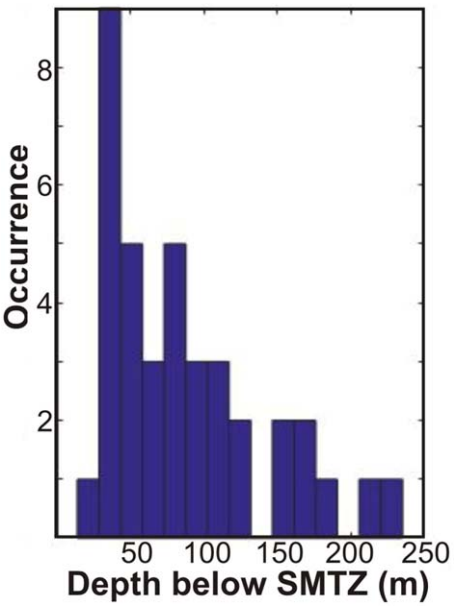

Figure 7. Distribution of the depth to the top of hydrate occurrence zone (TGHOZ) below the sulfate-methane transition zone (SMTZ) from all drilling campaigns listed in Table 1. The majority of sites show the first gas hydrates between 40 and 50 m below the SMTZ.

free lithology), especially if no core was recovered, or core hole and log-hole are at considerable distance to each other. In our analyses of correlations between the depth to the top and base of gas hydrate occurrence zone with the depth of the SMTZ and geothermal gradients, the uncertainties in the derived depth values vary between sites and are listed in Table 1.

In order to obtain a robust statistical analysis of the derived depths and geothermal gradients, we have used a total least squares (TLS) analytical technique, which allows variable errors in both dimensions and the definition of the robustness of the linear fit to the data with uncorrelated errors [*Krystek and Anton*, 2007]. Uncertainties used in the TLS method are dependent on the proxy used to define gas hydrate occurrence, as well as the statistical best fit value for defining BGHSZ (when e.g., using various measures from geophysical log-data, seismic, and thermal measurements). All uncertainties are included in Table 1.

3. Results

In general, drilling campaigns provide a wealth of information on the occurrence of gas hydrates and include analysis of local and regional geologic settings such as active continental margins with accretionary prisms (Cascadia, Nankai Trough) and erosive prisms (Costa Rica, Peru), passive continental margins (South China Sea, Blake Ridge, India, Gulf of Mexico, Borneo), and back-arc basins (Korea). None of the sites included in our compilation are associated with vigorous fluid flux at cold vents or other recent local disturbances such as sediment slumping.

As described in section 2 above, we have selected at each site listed in Table 1 the depth to the top of gas hydrate occurrence zone (TGHOZ), depth of the SMTZ, depth to the base of gas hydrate stability zone (BGHSZ) and the calculated geothermal gradient at the site, as determined either by using the cited values in the scientific literature or by reanalyzing the available data provided through the ODP and IODP online databases. Figure 4 combines observations in the relationship between measured geothermal gradients and the depths to the TGHOZ and BGHSZ. When plotting the BGHSZ depth values as function of depth below sea level (Figure 4a) assuming hydrostatic pressure conditions or meters below seafloor (Figure 4b), no obvious correlation with the geothermal gradients is evident. Similarly, with increasing thermal gradients, the TGHOZ should become shallower as methane becomes more soluble in the pore waters with increasing temperature, assuming constant upward fluid (including dissolved gas) flux rates from below. This trend is not obviously reflected in the drilling data (Figure 4c). However, there may be suggested lower limit for the TGHOZ for any given geothermal gradient (as shown by the dashed line in Figure 4c. The thickness of the gas hydrate occurrence zone is also not strongly correlated to the geothermal gradient values but the thickness is overall reduced with higher geothermal gradients (Figure 5).

As the occurrence of gas hydrate is closely linked to the site-specific shape of the methane solubility curve with depth and available methane in the subsurface to form gas hydrate (either from in situ microbial production or in combination with advection from fluids, where methane was generated at greater depth, including thermogenic sources), an initial thought has been, that the depth of the SMTZ may be an indicator for predicting the top of the first gas hydrate occurrence as it may reflect the in situ methane fluxes [*Bhatnagar et al.*, 2008, 2011; *Kastner et al.*, 2008; *Dickens and Snyder*, 2009; *Chatterjee et al.*, 2009; *Malinverno and Pohlman*, 2011]. An additional suggestion had been that there is a 1:10 relationship between the depths of the SMTZ and TGHOZ [*Paull et al.*, 2005]. On the basis of the available drilling data (Figure 6), we present three crossplots between the SMTZ depth and the depth of the TGHOZ and BGHSZ, as well as the thickness of the gas hydrate occurrence zone. As can be seen in the plots in Figure 6, the scatter in the complete data set is considerable and no clear trend for the entire data set can be identified. However, if for example only a sub-

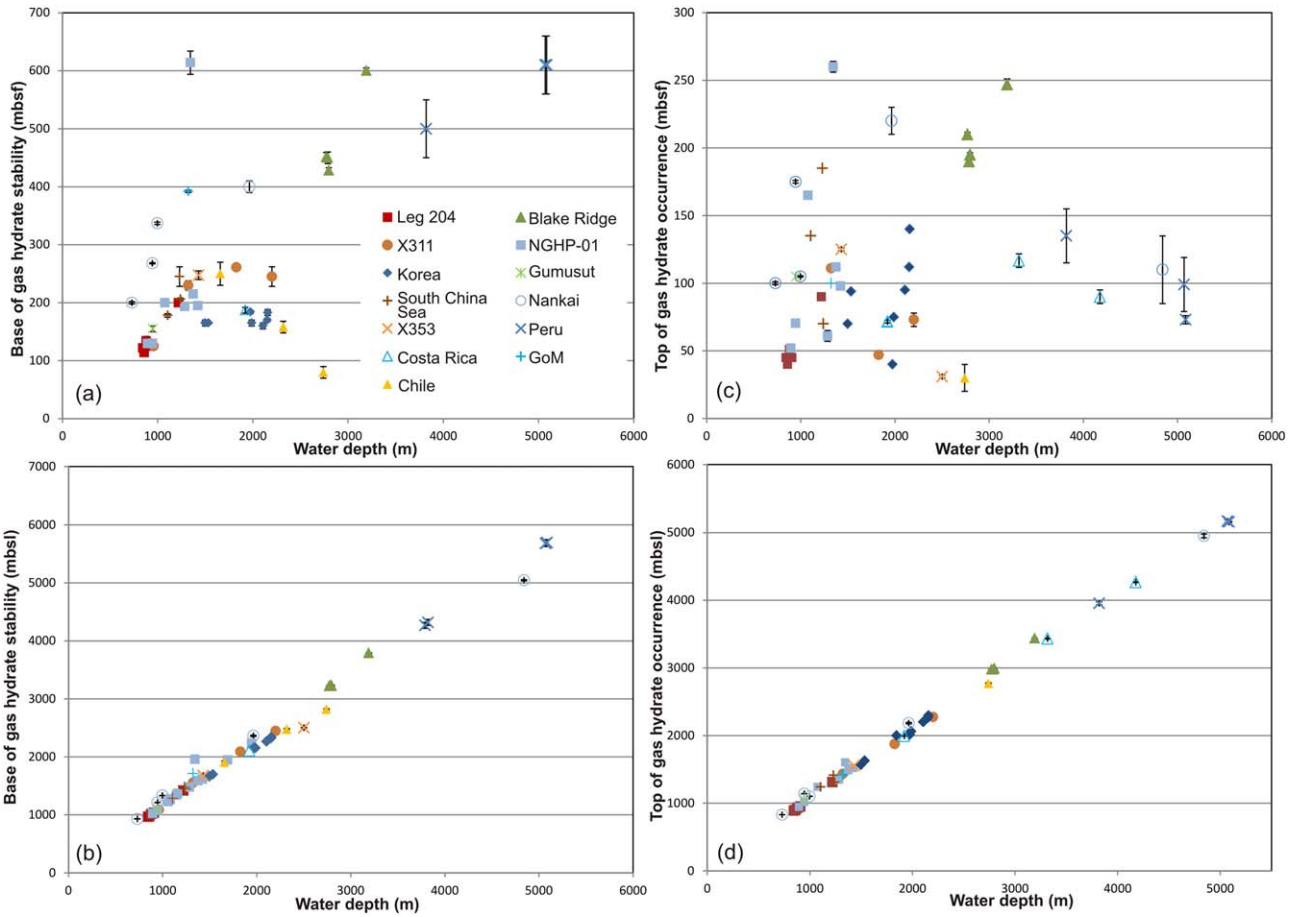

Figure 8. Correlations between water depth and (a, b) base of gas hydrate stability and (c, d) top of gas hydrate occurrence measured in meters below seafloor (mbsf, top) and meters below sea level (mbsl, bottom).

set of drill sites (e.g., only those from IODP Expedition 311) are used, some trend between the SMTZ and the depth to TGHOZ becomes evident, in that for a deeper SMTZ, the depth to the TGHOZ is increased, and the BGHSZ becomes shallower.

The depth of the base of the SMTZ is often very well defined through careful geochemical pore water and head-space gas analyses of core samples and the depth-uncertainty is overall small (∼0.5 m). Yet the uncertainty in assigning a value to the BGHSZ or TGHOZ may be as large as 10 m or even more for some of the sites from older drilling campaigns. Nonetheless, it is obvious from these data that the TGHOZ occurrence is not at the same depth as the base of the SMTZ but at some (often considerable) depth below (Figure 7). While the depth difference range between the TGHOZ and SMTZ is wide, ranging from 14 to 235 m, most sites cluster around a more narrow depth difference, ranging between 40 and 50 m.

Since the stability of gas hydrate in the sediments is dependent on the pressure regime, we further explore the potential relationships between water depth and the depth to the TGHOZ and the depth to the BGHSZ (Figure 8). Despite some scatter in the data, the expected trend of a deeper BGHSZ with greater water depth is evident in the crossplot of Figures 8a and 8b. While the depth to TGHOZ is weakly correlated with water depth when plotted as function of depth below seafloor (Figure 8c), the pressure dependence is also seen when plotting the depth to the TGHOZ as function of depth below sea level (Figure 8d). It clearly shows that the depth to the TGHOZ is a simple product of methane solubility related to pressure. In these analyses, there was little to no impact of gas flux or geothermal gradient at most sites. It is important to note, however, that we have not included high flux sites in this compilation. However, a quite notable exception from the otherwise rather linear trend seen in Figure 8d is Site NGHP01–17 drilled in the

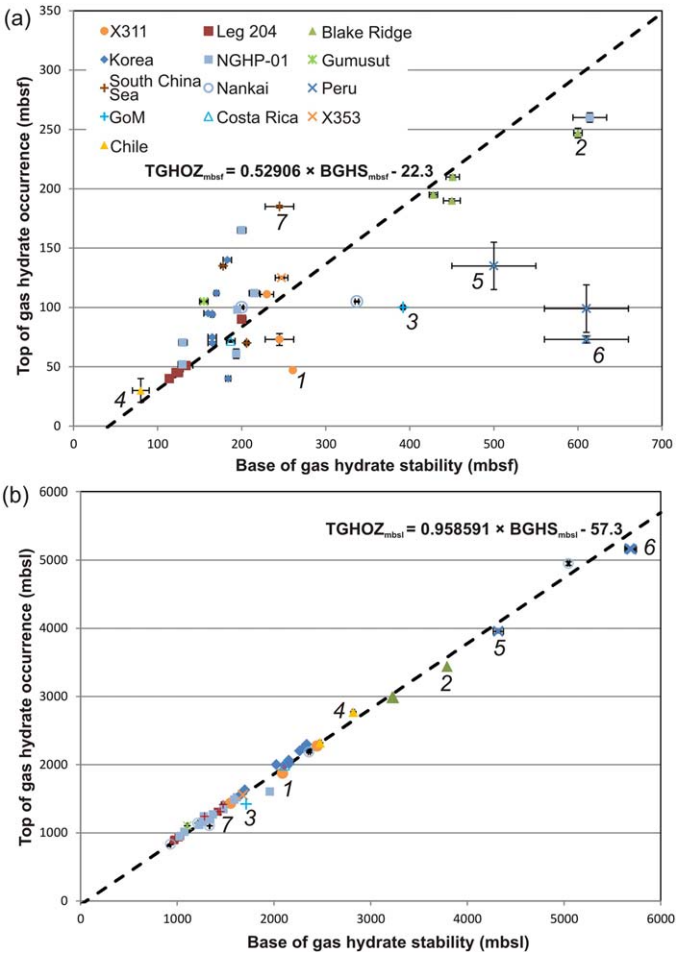

Figure 9. Correlation between the top of gas hydrate occurrence and base of gas hydrate stability measured in (a) meters below seafloor and (b) meters below sea level. Uncertainties (as defined in Table 1) are smaller than the symbol size used in Figure 8b. Seven examples of drill sites apparently randomly distributed in Figure 9a align according to water depth in Figure 9b (details see text).

Andaman Sea [*Collett et al*., 2014]. Here at a very low geothermal gradient of only 19°C/km and a water depth of 1344 m, gas hydrate was observed exclusively within ash layers.

Since formation of gas hydrates, their stability and thus overall occurrence within sediments are dependent on temperature and pressure conditions, there may be a correlation between these parameters themselves. Using the defined values for the depths to TGHOZ and the depth to the BGHSZ, two crossplots are shown in Figure 9 with both parameters measured in meters below the seafloor (Figure 9a) and meters below sea level (Figure 9b). While there is no strong correlation between the depth to TGHOZ and the depth to the BGHSZ when defined in meters below seafloor (simple regression yields an R^2 value of 0.5), a slightly stronger correlation exists if the sites off Peru are not included in the regression analysis. Using meters below sea level as measure for both parameters, a simple regression yields a high R^2 value of 0.8. Using the TLS method with uncertainties defined as in Table 1 (and no further weighting of input sites), we obtain as optimal liner fit:

$$TGHOZ_{mbsl} = 0.958591 \times BGHSZ_{mbsl} - 57.3 \quad (1)$$

The variance of the slope and intercept of equation (1) determined with TLS are 0.00000182 and 5.284564; or equivalently, the standard deviations are 0.001349 and 2.18, respectively.

However, this apparent linear behavior is also a consequence of having added to the small values of the depth to TGHOZ the values of water depth, which are roughly 1 order of magnitude larger than the value of TGHOZ measured in meter below seafloor. Yet when considering the placement of individual site pairings in depths to the TGHOZ and the depths to the BGHSZ, the correlation to water depth (i.e., hydrostatic pressure) is more easily understood. In Figure 9 we have selected seven such pairs (from IODP Expedition 311, South China Sea drilling, IODP Expedition 353 and ODP Leg 112) and show their placement in both crossplots to better demonstrate the relative movement of pairs from one to the other in each plots.

Instead of using the depth to the TGHOZ one may also construct a crossplot between the thickness of the gas hydrate occurrence zone (GHOZ) and the depth to the BGHSZ (Figure 10). Here a higher correlation is found when plotting the depth to the BGHSZ in meters below seafloor against thickness of the gas hydrate occurrence zone ($R^2 = 0.77$ with simple regression) than when using meters below sea level ($R^2 = 0.34$ with simple regression). Using TLS, we obtain as best linear fit:

$$\text{Thickness} = 0.737212125 \times \text{BGHSZ}_{\text{mbsf}} - 42.35 \quad (2)$$

The variance of the slope and intercept of equation (2) determined with TLS are 0.0000778 and 4.7409; or equivalently, the standard deviations are 0.00882 and 2.177, respectively. As seen above when considering full water depth ranges and top- and base of gas hydrate (Figures 8 and 9), the comparison of these two parameters is less meaningful when they are 1 order of magnitude apart (i.e., using meter below sea level instead of meter below seafloor). Thus, the apparently strongly linear correlations for crossplots using depth as meter below sea level may be rather misleading.

For completeness, we also show a crossplot of the thickness of the gas hydrate occurrence zone as function of the top of gas hydrate occurrence (Figure 11) as measured in meters below seafloor and meters below sea level. Here no obvious correlation is seen when considering the data measured in meters below seafloor (Figure 11a); however, if measured in meters below sea level a slightly linear trend may be evident between total thickness of gas hydrate occurrence and the top of first gas hydrate occurrence (Figure 11b).

Considering all parameters defined from these numerous drilling sites, we have placed the individual data on the gas hydrate phase-diagram in Figure 12, which assumes hydrostatic pressure conditions and uses temperature data from each site. Two scenarios of the gas hydrate phase boundary are included for seawater (35 ppt) and methane gas, and an arbitrary mix of 90% methane and 10% ethane (with seawater of 35 ppt). We also added previously published data [*Grevemeyer and Villinger*, 2001] to complete the data set, although some of these sites did not yield useable information for depth to the TGHOZ or the depth to the BGHSZ. Most plotted sites fall between the pure water and seawater gas (methane) hydrate stability boundaries. Some noticeable exceptions exist, as previously reviewed [*Ruppel*, 1997] for the sites on the Blake Ridge, where temperatures at the BGHSZ are lower than predicted using equilibrium conditions (pure seawater/methane).

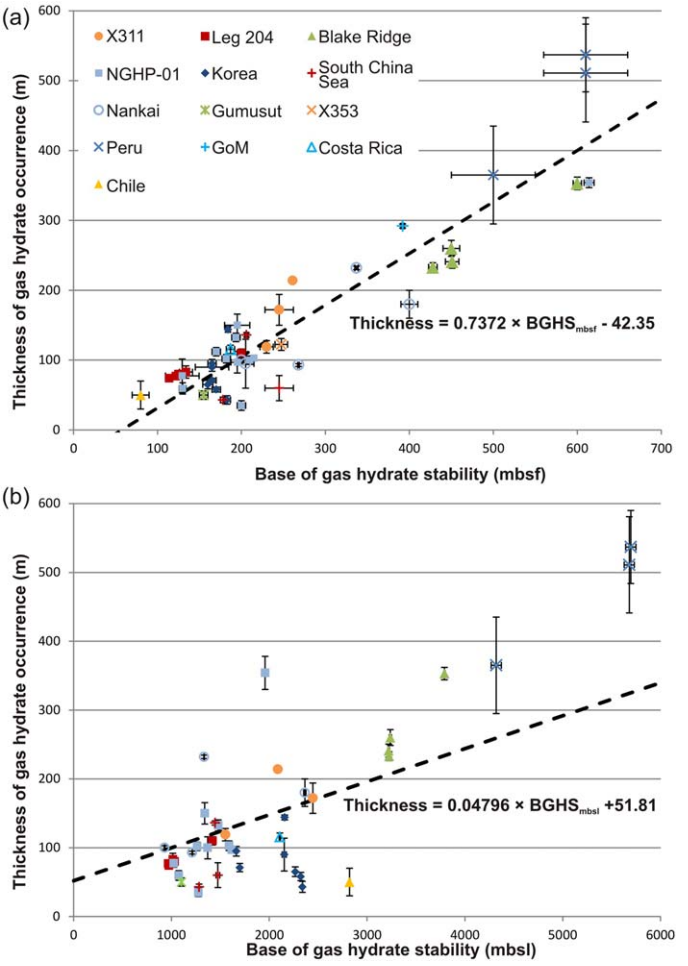

Figure 10. Correlations of the thickness of gas hydrate occurrence and base of gas hydrate stability measured in (a) meters below seafloor (mbsf) and (b) meters below sea level (mbsl). Uncertainties (Table 1) may be smaller than the symbol size used in some instances.

4. Discussion

The various crossplots shown in this study connect basic elements of gas hydrate occurrence and stability along the margins of numerous continents, providing valuable insights into the dynamics of the individual sites as well as an appreciation of elements common to most known marine gas hydrate occurrences.

It is not surprising to see no clear correlation between the depths of the SMTZ and any other parameter of the deeper gas hydrate system. This is in part discussed by *Kastner et al.* [2008] and *Dickens and Snyder* [2009] and relates to simplifying assumptions in the approach of using the shallow SMTZ characteristics for the deeper system. Issues

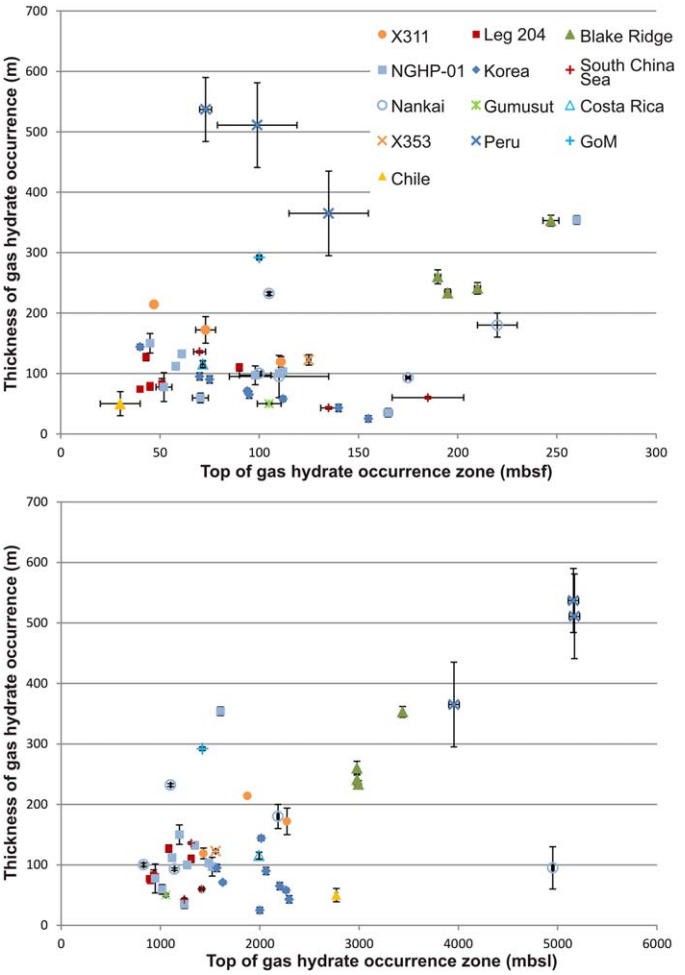

Figure 11. Correlations of the thickness of gas hydrate occurrence zone and the actual top of first gas hydrate occurrence measured in (a) meters below seafloor (mbsf) and (b) meters below sea level (mbsl). Uncertainties (Table 1) may be smaller than the symbol size used in some instances.

include assumptions of a purely vertical (1-D) fluid flux at the drill sites considered, no decoupling of the hydrologic and geologic systems by, e.g., mass wasting, and an assumption of steady state of the entire system over time.

Overall, the variation in the depth to the top of gas hydrate occurrence zone is significant and varies from a few tens of meters to slightly more than 250 mbsf. However, predicting the depth to the TGHOZ or GHOZ thickness either by using known (or estimated) values of the depth to the BGHSZ (e.g., from predrilling seismic information, or thermal modeling) may be done using either equation (1) or (2) that were derived from the crossplots shown in Figure 9b or 10a. Validating these two relationships may be done by comparing predicted and observed depths to the TGHOZ (Figure 13). Predicting the depth to the TGHOZ directly from the BGHSZ (in mbsl) shows that the majority of predictions are within 40 m of the observed values (Figure 13a, median value of 39.6), but some significant outliers are seen (e.g., from offshore Peru and Site NGHP-01–17 in the Andaman Sea). Using equation (2) to estimate the thickness of the GHOZ produces smaller errors overall (Figure 13b), with a median error of 29.8 m and smaller standard deviations, with the largest deviation seen only offshore Peru (where observations also had the largest uncertainties). Drilling along the margin off Peru as part of ODP Leg 112 was one of the first deep drilling expeditions where the recovery of gas hydrate was expected, but the analysis for the presence of gas hydrates during ODP Leg 112 was relatively less developed without the use of pressure coring or core temperature measurements. The depth uncertainty for TGHOZ is the largest in all of the compiled drilling campaigns and there was significant error in the assignment of the BSR depth for this site. As described by *Suess et al*. [1988], the BSR is not directly observed beneath Site 685 and Site 1230 of ODP Leg 201. A depth for the BGHSZ was defined from seismic data projecting BSR observations from nearby data by a distance of up to 5 km.

Another notable exception to the trends depicted in Figure 13a is Site NGHP-01–17 in the Andaman Sea. Here gas hydrate was almost exclusively observed in ash layers [*Rose et al*., 2013]. However, the very low thermal gradient of ~19°C/km results in a deep BGHSZ of >600 mbsf. Given a shallow water depth of ~1340 m, the depth to the TGHOZ is predicted to be deeper than 450 m with equation (1). Yet using equation (2) yields the thickness of the GHOZ within less than 60m (or ~15% of the observed value).

Given that the overall uncertainty in determining the depths to the TGHOZ and the depth to the BGHSZ (in some cases in excess of 10 m), especially at sites with incomplete core recovery or older vintage drilling prior to the use of IR and pressure-core technologies, the apparent relationship provided by both equations are reasonably well defined. Thus, they may be useful as first-order guides for regional and global estimates

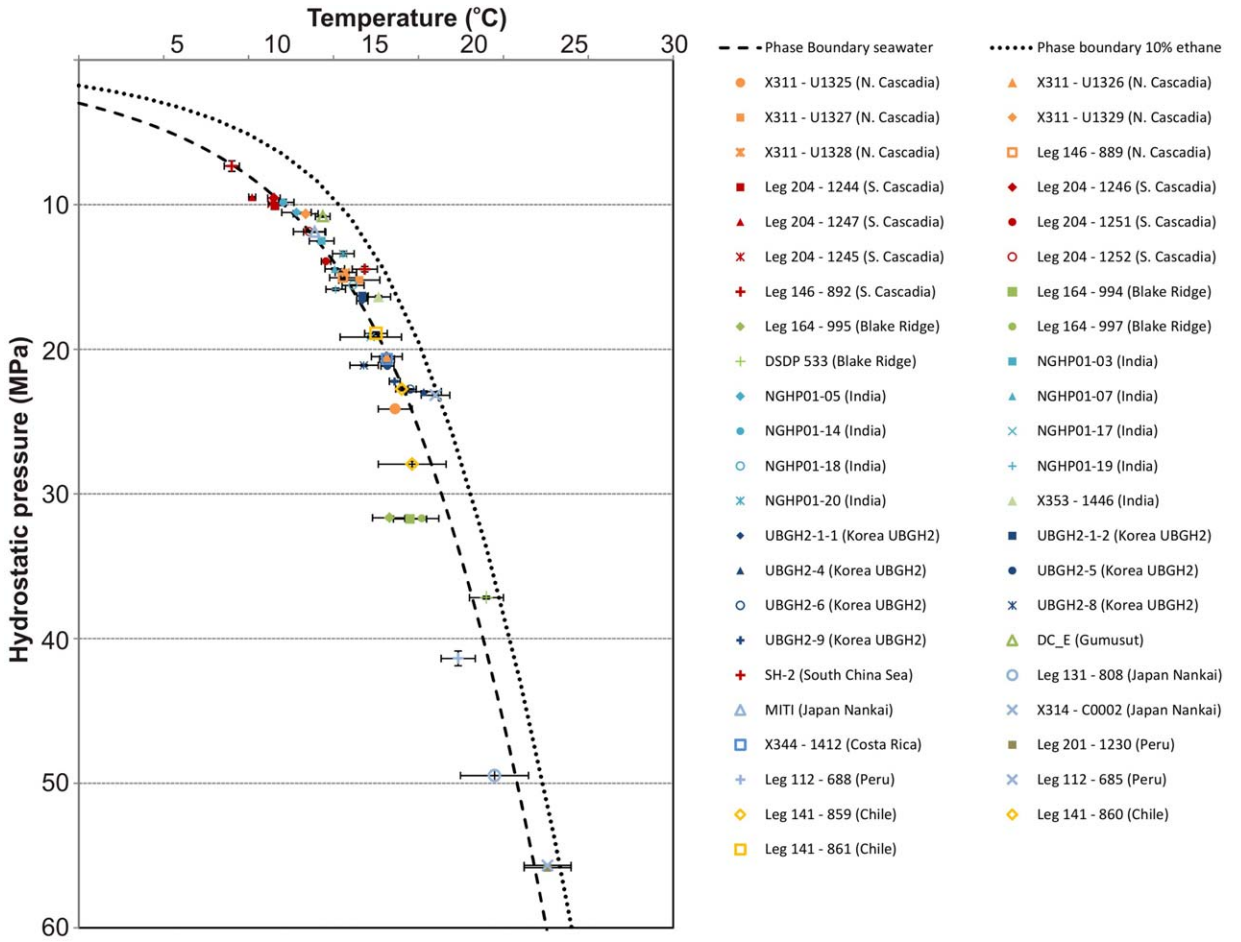

Figure 12. Phase-diagram for gas (methane only) hydrate stability. Shown are two lines for the phase boundary given seawater water of 35 ppt (dashed) and a mix of 10% ethane with 90% methane and seawater (dotted). Calculations were made using the hydrate prediction program called *hydoff* provided by *Sloan and Koh* [2008]. The program is available online at http://hydrates.mines.edu/CHR/Software.html. Additionally, sites reported in Table 1 with known pressure and temperature conditions from drilling at the base of gas hydrate stability and those reported by *Grevemeyer and Villinger* [2001] are included (Sites 889, 892, 859–861, 688, and 808). Error bars reflect uncertainties in the depth of the base of gas hydrate stability zone and geothermal gradients (Table 1).

of gas hydrate occurrence, or simply as planning tools for new drilling operations. Additionally, the data clearly confirm that gas hydrates (as defined from all these nonvent drill sites) occur at a significant depth below seafloor and well below the base of the SMTZ, which has some implications for climate-change scenarios, where seafloor warming (and associated sea level rise) is used to predict the dissociation of shallow gas hydrate deposits. It is important to note, however, our data is valid for only water depths within the range of drill sites surveyed for this study (i.e., 720–5090 m). The most critical depth zone for climate-change scenarios is likely shallower at 400–600 m water depth [e.g., *Ruppel*, 2011], but no scientific drilling has yet been conducted to verify gas hydrate occurrences within this critical zone. Thus, the relationships presented here should not be extended to regions outside their documented validity.

Reasons for the relatively uniform behavior and apparent applicability of correlations from using sites from many different margins around the world is likely to be found in the temperature dependence of methane solubility as the range in the derived geothermal gradients is rather limited. Further considerations in this discussion are (i) overall similarities in sedimentological settings of many of the sites which were drilled and cored through mostly mud-dominated sediments with few silt or sand interbeds associated with turbidities, (exception to this observation include Site NGHP01–17 were there are abundant coarse-grained ash layers also controlling the occurrence of gas hydrate, and Site U1326 offshore Vancouver Island, Canada, where a thick but shallow sequence of sandy turbidities was intersected), (ii) possibly similar amounts in total organic carbon to provide a potential source for gas in the system, and (iii) similar microbial activities that utilize this carbon to produce in situ methane.

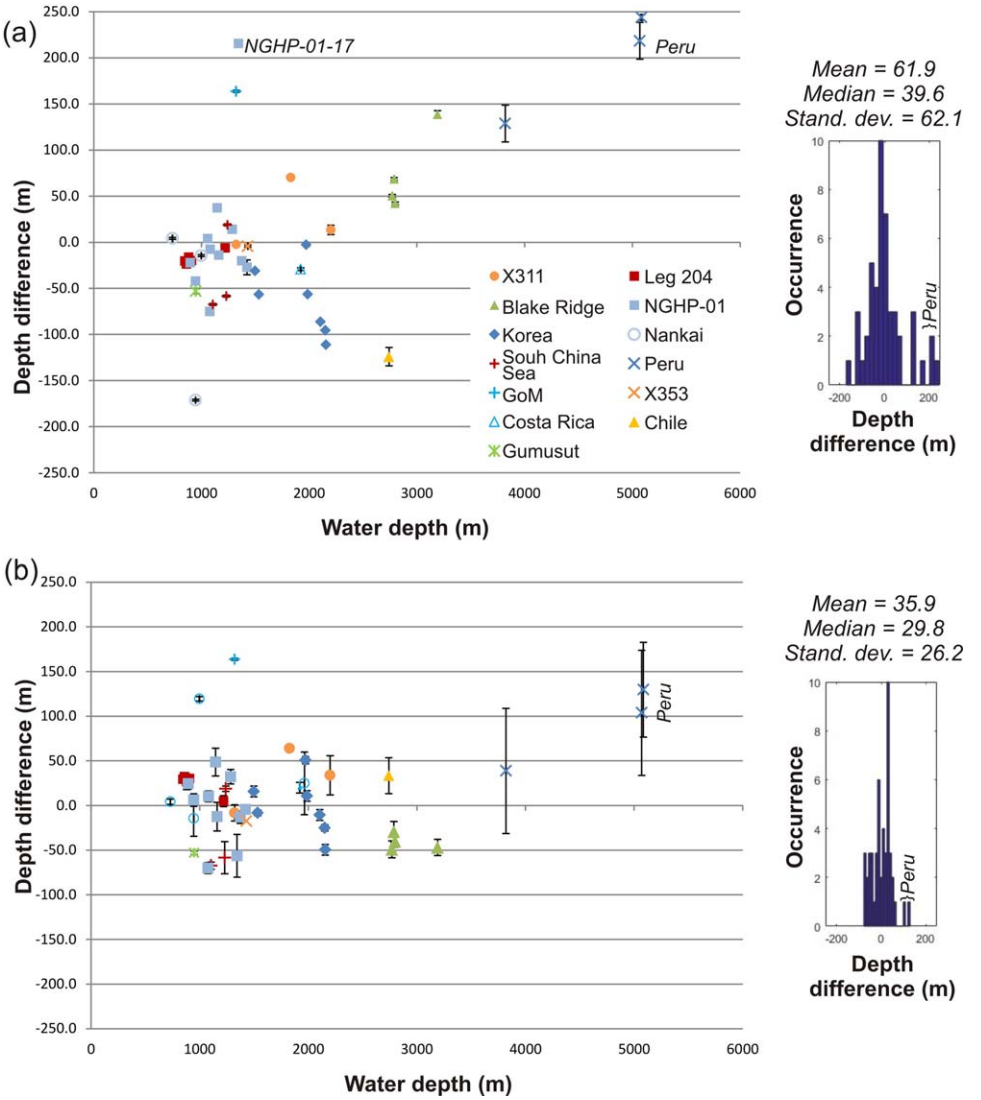

Figure 13. (a) Differences between predicated and observed values of top of gas hydrate occurrence zone (TGHOZ) using equation (1). (b) Differences between predicated and observed values of thickness in gas hydrate occurrence zone (GHOZ) using equation (2). In both diagrams, the uncertainties in defining TGHOZ or thickness of GHOZ are shown as defined in Table 1.

5. Conclusion

A global gas hydrate database was built in this study through the review of pertinent scientific drilling campaigns to create a compilation of a total of 58 drill sites completed as part of 21 drilling campaigns throughout the world. Sites compiled in this database do not include cold vent systems. Identifying and defining the depth limits of gas hydrate occurrences in this study was achieved by integrating inferred images of cores, pressure-core data, sedimentological texture-descriptions, core derived pore water freshening trends, and geophysical log-data (wireline or logging-while-drilling). Correlations between the measured depths of the sulfate-methane transition zone (SMTZ) and geothermal gradients did not yield any statistically significant trends. However, a first-order linear relationship between the top of gas hydrate occurrence zone (TGHOZ), and the depth to the base of gas hydrate stability zone (BGHSZ) was defined at each site examined in this study, when both parameters were referenced to the depth below sea level (i.e., as measured in meters below sea level). Despite the general difference of 1 order of magnitude between both values, a linear equation yields reasonably well-defined predictions for the depth to the TGHOZ that only deviate from the observed values for the majority of samples by less than 40 m. Similarly, the thickness of the gas hydrate occurrence zone (GHOZ) can be predicted reasonably well from the depth to the BGHSZ (defined in meters

below seafloor) where the difference between predicted and observed values is for most samples area less than 30 m (equivalent to <15% of the observed value).

The two depth correlations defined in this study from the compiled project database are only valid for the water depths of the drill sites surveyed in this study (720–5080 m) and thus may not be applicable for predicting gas hydrate occurrence along the up-slope "feather edge" of the gas hydrate stability zone in shallow water. Furthermore, these relationships are not intended to be used as gas hydrate exploration tools, but they do represent first-order estimates to predict the occurrence of conditions favorable for presence of gas hydrate in the subsurface. These relationships may be helpful as planning tools for new drilling campaigns, or as guide for global modeling of total gas hydrate abundance, or in scenarios of future global climate warming trends and linked release of methane from gas hydrate deposits.

Acknowledgments

This paper uses data from numerous drilling campaigns and we thank all those who contributed to the collection of data and publication of the research results we utilized in our compilation. Some samples and data used in this study were provided by the Integrated Ocean Drilling Program (IODP) and its predecessors Ocean Drilling Program (ODP) and Deep Sea Drilling Project (DSDP), which were funded by the U.S. National Science Foundation and participating countries under management of IODP Management International Inc. We thank the Captains and crews of the *JOIDES Resolution* and *Chikyu* as well as all technical staff for their support at sea for all DSDP, ODP, and IODP related data sets. All data from DSDP, ODP, and IODP expeditions are available online via the centralized International Ocean Drilling Data Archive (https://www.ngdc.noaa.gov/mgg/geology/drill.html) and links provided on that site. All other data used in this study are available through the publically available references. Any use of trade, product, or firm names is for descriptive purposes only and does not imply endorsement by the U.S. Government. Special thanks go to Florian Petersen for generating the map of Figure 2 with GMT. We also thank the anonymous reviewer for useful comments to our manuscript.

References

Bahk, J.-J., D.-H. Kim, J.-H. Chun, B.-K. Son, J.-H. Kim, B.-J. Ryu, M. E. Torres, M. Riedel, and P. Schultheiss (2013), Gas hydrate occurrences and their relation to host sediment properties: Results from Second Ulleung Basin Gas Hydrate Drilling Expedition, East Sea, *J. Mar. Pet. Geol.*, *47*, 21–29.

Behrmann, J. H., S. D. Lewis, R. J. Musgrave, and S. C. Cande (1992), *Proceedings of the Ocean Drilling Program, Initial Reports*, vol. 141, Ocean Drill. Program, College Station, Tex.

Bhatnagar, G., W. G. Chapman, G. R. Dickens, B. Dugan, and G. J. Hirasaki (2008), Sulfate-methane transition as a proxy for average methane hydrate saturation in marine sediments, *Geophys. Res. Lett.*, *35*, L03611, doi:10.1029/2007GL032500.

Bhatnagar, G., S. Chatterjee, W. G. Chapman, B. Dugan, G. R. Dickens, and G. J. Hirasaki (2011), Analytical theory relating the depth of the sulfate-methane transition to gas hydrate distribution and saturation, *Geochem. Geophys. Geosyst.*, *12*, Q03003, doi:10.1029/2010GC002297.

Booth, J. S., M. M. Rowe, and K. M. Fischer (1996), Offshore gas hydrate sample database with an overview and preliminary analysis, *U.S. Geol. Surv. Open File Rep.*, *96–272*, 31 pp.

Boswell, R., and T. S. Collett (2011), Current perspective on gas hydrate resources, *Energy Environ. Sci.*, *4*, 1206–1215, doi:10.1039/COEE00203H.

Boswell, R., C. Shipp, T. Reichel, D. Shelander, T. Saeki, M. Frye, W. Shedd, T. S. Collet, and D. R. McConnell (2016), Prospecting for marine gas hydrate resources, *Interpretation*, *4*(1), SA13–SA24, doi:10.1190/INT-2015-0036.1.

Chatterjee, S., G. Bhatnagar, W. G. Chapman, G. R. Dickens, B. Dugan, and G. J. Hirasaki (2009), Sulfate, methane, alkalinity, calcium and carbon isotope (d13C) profiles as an indicator of upward methane flux, *Eos Trans. AGU*, *90*(52), Fall Meet. Suppl., Abstract OS42A-05.

Clemens, S. C., W. Kuhnt, and L. J. LeVay, and the Expedition 353 Scientists (2016), *Proceedings of the International Ocean Discovery Program*, vol. 353, International Ocean Discovery Program (IODP), College Station, Tex., doi:10.14379/iodp.proc.353.105.2016.

Collett, T. S., and M. W. Lee (2012), Well log characterization of natural gas-hydrates, *Petrophysics*, *53*, 348–367.

Collett, T. S., et al. (2014), Geologic implications of gas hydrates in the offshore of India: Results of the National Gas Hydrate Program Expedition 01, *J. Mar. Pet. Geol.*, *58*, 3–28, doi:10.1016/j.marpetgeo.2014.07.021.

Davis, E. E., H. Villinger, R. D. MacDonald, R. D. Meldrum, and J. Grigel (1997), A robust rapid-response probe for measuring bottom-hole temperatures in deep-ocean boreholes, *Mar. Geophys. Res.*, *19*(3), 267–281.

D'Hondt, S. L., B. B. Jørgensen, D. J. Miller, and Shipboard Scientific Party (2003), *Proceedings of the Ocean Drilling Program, Initial Reports*, vol. 201, Ocean Drill. Program, College Station, Tex., doi:10.2973/odp.proc.ir.201.2003.

Dickens, G. R., and G. T. Snyder (2009), Interpreting upward methane flux from marine pore water profiles, in *Fire in the Ice, Winter*, pp. 7–10, Natl. Energy Technol. Lab., U.S. Dep. of Energy, Washington, D. C.

Ford, K. H., T. H. Naehr, and C. G. Skilbeck, and the Leg 201 Scientific Party (2003), The use of infrared thermal imaging to identify gas hydrate in sediment cores, in *Proceedings of Ocean Drilling Program, Initial Reports*, vol. 201, edited by S. L. D'Hondt et al., Ocean Drill. Program, 20 pp., College Station, Tex.

Grevemeyer, I., and H. Villinger (2001), Gas hydrate stability and the assessment of heat flow through continental margins, *Geophys. J. Int.*, *145*, 647–660.

Goldberg, D. S., R. L. Kleinberg, J. L. Weinberger, A. Malinverno, P. J. McLellan, and T. S. Collett (2010), Evaluation of natural gas-hydrate systems using borehole logs, in *Geophysical Characterization of Gas Hydrates: SEG Geophysical Developments Series 1*, vol. 4, edited by M. Riedel, E.C. Willoughby, and S. Chopra, pp. 239–261, Tulsa, Okla.

Harris, R. N., A. Sakaguchi, and K. Petronotis, and the Expedition 344 Scientists (2013), *Proceedings of the Integrated Ocean Drilling Program*, vol. 344, Integr. Ocean Drill. Program, College Station, Tex., doi:10.2204/iodp.proc.344.2013.

Heesemann, M., H. Villinger, A. T. Fisher, A. M. Tréhu, and S. Witte (2006), Data report: Testing and development of the new APC3 tool to determine in situ temperatures while piston coring, in *Proceedings of the Integrated Ocean Drilling Program*, vol. 311, edited by M. Riedel et al., 19 pp., Integr. Ocean Drill. Program Manage. Int., Inc., Washington, D. C., doi:10.2204/iodp.proc.311.108.2006.

Hesse, R., and W. E. Harrison (1981), Gas hydrates (clathrates) causing pore-water freshening and oxygen isotope fractionation in deep-water sedimentary sections of terrigenous continental margins, *Earth Planet. Sci. Lett.*, *55*, 453–462.

Kastner, M., K. A. Kvenvolden, M. J. Whiticar, A. Camerlenghi, and T. D. Lorenson (1995), Relation between pore fluid chemistry and gas hydrates associated with bottom-simulating reflectors at the Cascadia margin, Sites 889 and 892, in *Proceedings of the Ocean Drilling Program, Scientific Results, Part 1*, vol. 146, edited by B. Carson et al., Ocean Drill. Program, pp. 175–187, College Station, Tex.

Kastner, M., M. E. Torres, E. A. Solomon, and A. J. Spivack (2008), Marine pore fluid profiles of dissolved sulfate: Do they reflect in situ methane fluxes?, in *Fire in the Ice, Summer*, pp. 6–8, Natl. Energy Technol. Lab., U.S. Dep. of Energy, Washington, D. C.

Kimura, G., E. Silver, and P. Blum, and Shipboard Scientific Party (1997), *Proceedings of the Ocean Drilling Program, Initial Reports*, vol. 170, Ocean Drill. Program, College Station, Tex.

Klauda, J. B., and S. I. Sandler (2005), Global distribution of methane hydrate in ocean sediment, *Energy Fuels*, *19*, 459–470.

Krystek, M., and M. Anton (2007), A weighted total least-squares algorithm for fitting a straight line, *Meas. Sci. Technol.*, *18*(11), 3348–3442.

Kumar, P., et al. (2014), Geologic implications of gas hydrates in the offshore of India: Krishna-Godavari Basin, Mahanadi Basin, Andaman Sea, Kerola-Konkan Basin, *J. Mar. Pet. Geol.*, *58*, Part A, 29–98, doi:10.1016/j.marpetgeo.2014.07.031.

Kvenvolden, K. A. (1988), Methane hydrate—A major reservoir of carbon in the shallow geosphere?, *Chem. Geol.*, *71*(1–3), 41–51.

Kvenvolden, K. A., and T. D. Lorenson (2001), The global occurrence of natural gas hydrate, in *Natural Gas Hydrates—Occurrence, Distribution, and Detection*, edited by C. K. Paull and W. P. Dillon, pp. 3–18, AGU, Washington, D. C.

Long, P., M. Holland, P. Schultheiss, M. Riedel, J. Weinberger, A. Tréhu, and H. Schaef (2010), Infrared (IR) imaging of gas hydrate-bearing cores: State-of-the-art and future prospects, in *Geophysical Characterization of Gas Hydrates: SEG Geophysical Developments Series 14*, edited by M. Riedel, E. C. Willoughby, and S. Chopra, pp. 217–231, Tulsa, Okla.

Malinverno, A., and J. W. Pohlman (2011), Modeling sulfate reduction in methane hydrate-bearing continental margin sediments: Does a sulfate methane transition require anaerobic oxidation of methane?, *Geochem. Geophys. Geosyst.*, *12*, Q07006, doi:10.1029/2011GC003501.

Marquardt, M., C. Hensen, E. Pinero, K. Wallmann, and M. Haeckel (2010), A transfer function for the prediction of gas hydrate inventories n marine sediments, *Biogeosciences*, *7*, 2925–2941, doi:10.5194/bg-7-2925-2010.

Matsumoto, R. (2008), Geochemical proxies and temperature regimes for the distribution of gas hydrates in Nankai Trough, paper presented at the AAPG Hedberg Conference on Gas Hydrates: Energy Resource Potential and associated Geologic Hazards, American Association of Petroleum Geologists (AAPG), Vancouver, B. C., Canada.

Matsumoto, R., B.-J. Ryu, S.-R. Lee, S. Lin, S. Wu, K. Sain, I. Pecher, and M. Riedel (2011), Occurrence and exploration of gas hydrate in the marginal seas and continental margin of the Asia and Oceania region, *J. Mar. Pet. Geol.*, *28*, 1751–1767, doi:10.1016/j.marpetgeo.2011.09.009.

Milkov, A. V. (2003), Global estimates of hydrate-bound gas in marine sediments: How much is really out there?, *Earth Sci. Rev.*, *66*(3–4), 183–197, doi:10.1016/j.earscirev.2003.11.002.

Minerals Management Service (2008), Preliminary evaluation of in-place gas hydrate resources: Gulf of Mexico Outer Continental Shelf, *OCS Rep. MMS, 2008–004*, 136 pp.

Miyakawa, A., S. Saito, Y. Yamada, H. Tomaru, M. Kinoshita, and T. Tsuji (2014), Gas hydrate saturation at Site C0002, IODP Expeditions 314 and 315, in the Kumano Basin, Nankai Trough, *Isl. Arc*, *23*, 142–156.

Paganoni, M., J. A. Cartwright, M. Foschi, R. C. Shipp, and P. Van Rensbergen (2016), Structure II gas hydrates found below the bottom-simulating reflector, *Geophys. Res. Lett.*, *43*, 5696–5706, doi:10.1002/2016GL069452.

Park, K.-P., J.-J. Bahk, Y. Kwon, G. Y. Kim, M. Riedel, M. Holland, P. Schultheiss, and K. Rose, and the UBGH-1 Scientific Party (2008), *Korean National Program Expedition Confirms Rich Gas Hydrate Deposit in the Ulleung Basin, East Sea, NETL Newsletter "Fire in the Ice,"* Spring 2008, NETL, Pittsburgh, Pa. [Available at http://www.netl.doe.gov/MethaneHydrates.]

Paull, C. K., R. Matsumoto, P. J. Wallace, et al. (1996), *Proceedings of the Ocean Drilling Program, Initial Reports*, vol. 164, Ocean Drill. Program, College Station, Tex.

Paull, C. K., W. Ussler III, T. Lorenson, W. Winters, and J. Dougherty (2005), Geochemical constraints on the distribution of gas hydrates in the Gulf of Mexico, *Geo Mar. Lett.*, *25*(5), 273–280, doi:10.1007/s00367-005-0001-3.

Pinero, E., E. Gracia, F. Martinez-Ruiz, J. C. Larrasoana, A. Vizcaino, and G. Ercilla (2007), Gas hydrate disturbance fabrics of southern Hydrate Ridge sediments (ODP Leg 204): Relationship with texture and physical properties, *Geo Mar. Lett.*, *27*(2), 279–288.

Riedel, M., T. S. Collett, and M. J. Malone, and the Expedition 311 Scientists (2006), *Proceedings of the Integrated Ocean Drilling Program*, vol. 311, Integr. Ocean Drill. Program Manage. Int., Inc., Washington, D. C., doi:10.2204/iodp.proc.311.2006.

Riedel, M., E. C. Willoughby, and S. Chopra (2010), Geophysical characterization of gas hydrates, *Geophys. Dev. 14*, Soc. of Explor. Geophys., 385 pp., Tulsa, Okla.

Rose, K. K., J. E. Johnson, M. E. Torres, W.-L. Hong, L. Giosan, E. Solomon, M. Kastner, T. Cawthern, P. E. Long, and T. Schaef (2013), Anomalous porosity preservation and preferential accumulation of gas hydrate in the Andaman accretionary wedge, NGHP-01 site 17A, *J. Mar. Pet. Geol.*, *58*, Part A, 99–116, doi:10.1016/j.marpetgeo.2014.04.009.

Ruppel, C. (1997), Anomalously cold temperatures observed at the base of the gas hydrate stability zone, U.S. Atlantic passive margin, *Geology*, *25*, 699–702.

Ruppel, C., R. Boswell, and E. Jones (2008), Scientific results from Gulf of Mexico Gas Hydrates Joint Industry Project Leg 1 drilling: Introduction and overview, *J. Mar. Pet. Geol.*, *25*, 819–829, doi:10.1016/j.marpetgeo.2008.02.007.

Ruppel, C. D. (2011), Methane hydrates and contemporary climate change, *Nat. Educ. Knowledge*, *3*(10), 29.

Ryu, B.-J., T. S. Collett, M. Riedel, G.-Y. Kim, J.-H. Chun, J.-J. Bahk, J.-Y. Lee, J.-H. Kim, and D.-G. Yoo (2013), Scientific results of the second gas hydrate drilling expedition in the Ulleung Basin (UBGH2), *J. Mar. Pet. Geol.*, *47*, 1–20.

Schultheiss, P., M. Holland, and F. Rack (2010), Borehole pressure coring techniques and core analysis at in situ pressure, in *Geophysical Characterization of Gas Hydrates, SEG Geophys. Dev. Ser. 14*, edited by M. Riedel, E. C. Willoughby, and S. Chopra, pp. 263–278.

Sheridan, R. E., et al. (1983), *Initial Reports Deep Sea Drilling Project*, vol. 76, U.S. Gov. Print. Off., Washington, D. C., doi:10.2973/dsdp.proc.76.1983.

Sloan, E. D., and C. A. Koh (2008), *Clathrate Hydrates of Natural Gases*, 3rd ed., 720 pp., Taylor and Francis, Boca Raton, Fla.

Suess, E., and R. von Huene, and Shipboard Scientific Party (1988), *Proceedings of the Ocean Drilling Program, Initial Reports*, vol. 112, Ocean Drill. Program, College Station, Tex.

Taira, A., I. Hill, and J. Firth, and Shipboard Scientific Party (1991), *Proceedings of the Ocean Drilling Program, Initial Reports*, vol. 131, Ocean Drill. Program, College Station, Tex.

Takeuchi, R., and R. Matsumoto (2009), Geological and geochemical constraints on the process of gas hydrate formation and accumulation in the Eastern Nankai Trough, off Central Japan [in Japanese, with English abstract], *J. Geogr.*, *118*(5), 793–813.

Tréhu, A. M., G. Bohrmann, F. R. Rack, M. E. Torres, et al. (2003), *Proceedings of the Ocean Drilling Program, Initial Reports*, vol. 204, Ocean Drill. Program, College Station, Tex., doi:10.2973/odp.proc.ir.204.2003.

Tréhu, A. M., et al. (2004), Three-dimensional distribution of gas hydrate beneath southern Hydrate Ridge: Constraints from ODP Leg 204, *Earth Planet. Sci. Lett.*, *227*(2004), 557–558.

Tsuji, Y., H. Ishida, M. Nakamizu, R. Matsumoto, and S. Shimizu (2004), Overview of the MITI Nankai Trough Wells: A milestone in the evaluation of methane hydrate resources, *Resour. Geol.*, *54*(1), 3–10, doi:10.1111/j.1751-3928.2004.tb00182.x.

Wallmann, K., G. Aloisi, M. Haeckel, A. Obzhirov, G. Pavlova, and P. Tishchenko (2006), Kinetics of organic matter degradation, microbial methane generation, and gas hydrate formation in anoxic marine sediments, *Geochim. Cosmochim. Acta*, *70*, 3905–3927.

Wang, X., S. Wu, M. Lee, Y. Guo, S. Yang, and J. Liang (2011a), Gas hydrate saturation from acoustic impedance and resistivity logs in the Shenhu area, South China Sea, *J. Mar. Pet. Geol.*, *28*, 1625–1633, doi:10.1016/j.marpetgeo.2011.07.002.

Wang, X., S. Wu, S. Yang, J. Liang, Y. Guo, Y. Gong, and D. R. Hutchinson (2011b), Gas hydrate occurrence, saturations, and geophysical signatures associated with fluid flow in silt-dominated reservoirs in the northern South China Sea, paper presented at the 7th International Conference on Gas Hydrates, 17–21 July, Edinburgh, U. K. [Available at www.pet.hw.ac.uk/icgh7/papers/icgh2011Final00108.pdf.]

Wang, X., M. Lee, T. S. Collett, S. Yang, Y. Guo, and S. Wu (2014a), Gas hydrate identified in sand-rich inferred sedimentary section using downhole logging and seismic data in Shenhu area, South China Sea, *J. Mar. Pet. Geol.*, *51*, 298–306, doi:10.1016/j.marpetgeo.2014.01.002.

Wang, X., T. S. Collett, M. W. Lee, S. Yang, Y. Guo, and S. Wu (2014b), Geological controls on the occurrence of gas hydrate from core, downhole log, and seismic data in the Shenhu area, South China Sea, *J. Mar. Pet. Geol.*, *357*, 272–292, doi:10.1016/j.margeo.2014.09.040.

Weinberger, J. L., K. M. Brown, and P. E. Long (2005), Painting a picture of gas hydrate distribution with thermal images, *Geophys. Res. Lett.*, *32*, L04609, doi:10.1029/2004GL021437.

Westbrook, G. K., B. Carson, R. J. Musgrave, et al. (1994), *Proceedings of the Ocean Drilling Program, Initial Reports*, vol. 146, Part 1, Ocean Drill. Program, College Station, Tex.

Wu, N., H. Zhang, S. Yang, G. Zhang, J. Liang, J. Lu, X. Su, P. Schulheiss, M. Holland, and Y. Zhu (2011), Gas hydrate system of Shenhu Area, Northern South China Sea: Geochemical results, *J. Geol. Res.*, *2011*, 370298, doi:10.1155/2011/370298.

Xu, W., and C. Ruppel (1999), Predicting the occurrence, distribution, and evolution of methane gas hydrate in porous marine sediments from analytical models, *J. Geophys. Res.*, *104*(B3), 5081–5096.